

Received October 30, 2020, accepted November 19, 2020, date of publication November 24, 2020, date of current version December 10, 2020.

Digital Object Identifier 10.1109/ACCESS.2020.3039996

# A New Trend of Quantum Image Representations

JIE SU<sup>1</sup>, XUCHAO GUO, CHENGQI LIU, AND LIN LI

College of Information and Electrical Engineering, China Agricultural University, Beijing 100083, China

Corresponding author: Lin Li (lilinli@cau.edu.cn)

This work was supported by the National Key Research and Development Project of China under Grant 2016YFD0300710.

**ABSTRACT** Quantum image processing will be an important issue in the age of quantum computers. Quantum image processing generally includes quantum image representations, quantum image processing algorithms, and quantum image measurement. Among them, quantum image representation is a very important part of quantum image processing. Therefore, it is of great significance for quantum image processing to study the representation of quantum images. First, we elaborate on the main quantum image representations and analyze, compare and summarize them. This paper focuses on the definition of these quantum image representations the preparation of quantum images and the number of quantum bits required as well as the computational complexity. Then, this paper analyzes, compares and summarizes the similarities and differences between these quantum image representations. Finally, the challenges and future development in the field of quantum image processing are summarized and forecasted. This work will help researchers to understand the advances related to quantum image representations in the field of quantum image processing and is therefore of some reference value.

**INDEX TERMS** Quantum algorithms, quantum computation, quantum image representation, quantum image processing, quantum information.

## I. INTRODUCTION

Different quantum images can achieve different quantum image processing purposes. Based on a variety of quantum physical devices, the complication and representation of quantum images have become very urgent research in the field of quantum image processing. At present, some scholars have carried out relevant analyses and discussions on quantum image representation, which has promoted the development of this field [1]. How to extend the image processing and operations in the classical domain to the quantum computing framework is the research focus in the field of quantum image processing. In 2003, Venegas-Andraca and Bose proposed the Qubit Lattice quantum image representation [2]. Later, Latorre *et al.* proposed the quantum representation called Real Ket. Le *et al.* proposed and revised the FRQI (Flexible Representation of Quantum Images) [3], [4]. These three representations have become classics in the field of quantum image and have performed well in image storage and acquisition [5], [6]. Among them, the FRQI uses the normalized state to store the position information and color information of each pixel in the image, which greatly

reduces the qubits needed in the process of quantum image preparation. Besides, the FRQI can realize the geometric transformation and color transformation of images at the same time. Therefore, it has attracted the attention of many research fields, such as image database retrieval, quantum watermarking technology, quantum movie technology, and other application fields [7]–[13].

In 2016, F. Yan *et al.* published a survey on quantum image representations [1]. That survey gathered eight mainstream quantum image representations (QIRs) and discussed the advances made in the area before 2016. Also, that survey reviewed some similarities, differences, and likely applications for some of the available QIRs. However, with the development of recent years, quantum image representations have been expanded to some extent. Therefore, it is necessary to survey the quantum image representations further.

Inspired by the three representations, a series of new quantum image representations have appeared. At present, quantum image representations mainly include NAQSS (Normal Arbitrary Quantum Superposition State) [14], QSMC&QSNC (Quantum States for M Colors and N Coordinates of An Image) [15], SQR (Simple Quantum Representation of Infrared Images) [16], QUALPI (Quantum Log-Polar Images) [17], NEQR (Novel Enhanced

The associate editor coordinating the review of this manuscript and approving it for publication was Sun Junwei<sup>1</sup>.

Quantum Representation) [18], CQIR (Caraiman’s Quantum Image Representation) [19], MCQI (Multi-Channel Quantum Images) [20], INEQR(Improved NEQR) [21], GNEQR(A Generalized Model of NEQR) [22], NCQI(A Novel Quantum Representation of Color Digital Images) [23], BRQI (A Bitplane Representation of Quantum Images) [24], QRCI(A New Quantum Representation Model of Color Digital Images) [25], QRMMI (A Quantum Representation Model for Multiple Images) [26], QRMW (Quantum Representation of Multi Wavelength Images) [27], OCQR (An Optimized Quantum Representation for Color Digital Images) [28], FRQCI (An Improved FRQI Model) [29], QMCR (A Digital RGB Multi-Channel Representation for Quantum Colored Images) [30], IFRQI (Improved Flexible Representation of Quantum Images) [31], QBIR (A Quantum Block Image Representation) [32], OQIM (Order-encoded Quantum Image Model) [33], QIIR (Quantum Indexed Image Representation) [8], and DRQCI (A Double Quantum Color Images Representation Model) [34].

The spectrum includes the visible spectrum and the invisible spectrum, and an image can be generated by detecting its energy. In the field of quantum images, how to construct the corresponding quantum image representation to store the image information carried by the spectral energy is the most basic step. In order to store image information, a function mapping-like device is first needed to convert spectral energy values into quantum states [2]. Then, the index of the energy detector array is adjusted according to the visual information effect of the whole quantum image, thereby storing the image in the quantum image representation model. In the following sections, the above quantum image representations are mainly introduced.

## II. QUANTUM IMAGE REPRESENTATION AND ITS SUMMARY

Quantum computing is a product of the combination of quantum mechanics and computer science, and it is a new computational paradigm that has emerged as a possible solution to the Moore’s Law failure problem. In image processing, the storage, processing and retrieval of images are the main tasks. In a classical computer, the pixels and coordinates of an image are stored in mutually independent bits in the computer. If one part of the image has important correlations with other parts, the classical computer has to use extra space to store these correlations, otherwise, these correlations will be lost. Therefore, storing images in classical computers requires a large amount of storage space, and this storage mechanism has an impact on the parallel computing performance of the images. Quantum computing has inherent properties such as quantum coherence, entanglement, and superposition of quantum states, and this unique computational performance makes quantum computing superior to classical computing in terms of information storage and parallel computation. Therefore, we can use a combination of quantum computing and image processing to improve the image processing effect and computational performance [35]. In a quantum computer,

an image can be represented as a superposition of quantum bits, and the number of quantum bits required is much smaller than the number of bits required for a classical image [36]. When the task of real-time processing of large-scale images is required, the quantum representation of the image to utilize a quantum computer for processing can improve processing efficiency.

The goal of quantum image processing is to use quantum computing technology to realize the operation of different image formats to achieve various practical purposes [5]. The quantum image representations used are different for different purposes. Next, some important quantum image representations are described, among which the definition and description of these representations come from a series of references.

### A. FRQI

Inspired by the pixel representation for images in conventional computers, FRQI was proposed. FRQI is an image representation in the form of a standardized state on a quantum computer. The FRQI compiles and converts color information and position information of image into a quantum state according to the method of classical image representation [3], [4]. Its formula is shown below:

$$|I\rangle = \frac{1}{2^n} \sum_{i=0}^{2^{2n}-1} |c_i\rangle \otimes |i\rangle, \quad (1)$$

where  $\otimes$  is the tensor product notation and

$$|c_i\rangle = \cos \theta_i |0\rangle + \sin \theta_i |1\rangle. \quad (2)$$

In Eq. (2),  $|0\rangle$  and  $|1\rangle$  are two-dimensional quantum base states.  $|i\rangle$  is  $2n$ -dimensional quantum state.  $i = 0, 1, \dots, 2^{2n} - 1$ ,  $\theta_i \in [0, \pi/2]$  and  $\theta = (\theta_0, \theta_1, \dots, \theta_{2^{2n}-1})$ .  $\theta$  is the angle vector corresponding to the color information. In the FRQI, it mainly includes 0 and 1, which are used to compile the color information and position information of the image, respectively.

In practical application, for example, a  $2 \times 2$  image and its FRQI state are shown in FIGURE 1.

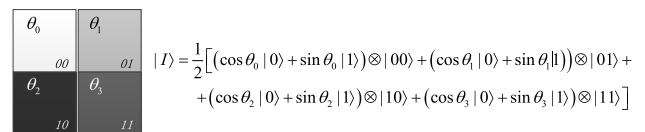


FIGURE 1. A  $2 \times 2$  FRQI quantum image and its quantum state.

The polynomial preparation theorem (PPT) as developed by using Theorem 1 shows a constructively efficient implementation of the preparation process.

*Theorem 1:* Given a vector  $\theta = (\theta_0, \theta_1, \dots, \theta_{2^{2n}-1})$  ( $n \in \mathbb{N}$ ) of angles, there is a unitary transform  $\mathcal{P}$  that turns quantum computers from the initialized state,  $|0\rangle^{\otimes 2n+1}$ , to the FRQI state in Eq. (1), composed by Hadamard and controlled rotation transforms [3].

*Proof:* From the proof of [3].

Therefore, the unitary transformation is the transform turning quantum computers from the initialized state  $|0\rangle^{\otimes 2n+1}$  to the FRQI state. Therein, the computational complexity of the whole preparation for FRQI could be calculated as  $O(2^{4n})$ .

FRQI has the advantage of quantum superposition states in which the quantum states of the stored image are normalized. However, FRQI does not support color images, is not suitable for local image transformations, and does not allow for accurate image measurements.

### B. NAQSS

Multi-dimensional color image processing has two difficulties: One is that a large number of bits are needed to store multi-dimensional color images, such as a three-dimensional color image of  $1024 \times 1024 \times 1024$  needs  $1024 \times 1024 \times 1024 \times 24$  bits. The other one is that the efficiency or accuracy of image segmentation is not high enough for some images to be used in a content-based image search. To solve the above problems, NAQSS was proposed. The NAQSS is a  $(n + 1)$ -qubit quantum representation, which can be used to represent multi-dimensional color images [14]. The first  $n$  bits of the NAQSS are used to represent the coordinates of  $2^n$  pixels, and the remaining bit represents the segmentation information of the image. The NAQSS corresponds to the color and angle of the image one to one, mapping the color information to a certain value on the interval  $[0, \pi/2]$ . The NAQSS can be represented as

$$|I\rangle = \sum_{i=0}^{2^n-1} \theta_i |v_1\rangle |v_2\rangle \cdots |v_k\rangle \otimes |\chi_i\rangle, \quad (3)$$

where

$$|\chi_i\rangle = \cos \gamma_i |0\rangle + \sin \gamma_i |1\rangle. \quad (4)$$

Eq. (4) is used to represent the segmentation information of an image. If the image is divided into  $m$  sub-images,  $\gamma_i$  can establish a corresponding relationship  $m$  by constructing a bijective function. Among them, the pixel points contained in each sub-image can be represented by the coordinate  $|v_1\rangle |v_2\rangle \cdots |v_k\rangle$ .

In practical application, for example, a  $2 \times 2 \times 2$  NAQSS quantum image with its quantum state is shown in FIGURE 2.

NAQSS can satisfy multi-dimensional color image processing and improve the efficiency and accuracy of image

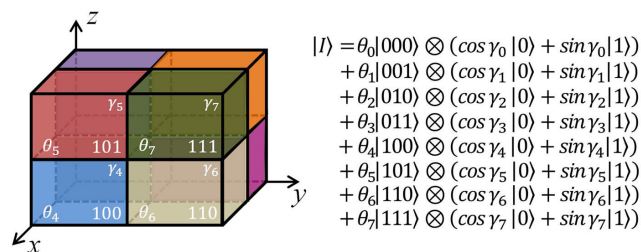


FIGURE 2. A  $2 \times 2 \times 2$  NAQSS quantum image and its quantum state (figure adapted from [14]).

segmentation. However, it cannot accurately measure the pixels of the image.

The circuit of NAQSS is built with  $(2^{n+1} - 1)$  quantum gates which can be constructed by one-bit and two-bit gates whose total number is  $o(N \log^2 N)$  where  $N = 2^n$  is the pixel's number of an image. For detailed proof of the computational complexity, see Ref. [14].

### C. QSMC&QSNc

The QSMC&QSNc uses the two sets of quantum states QSMC and QSNc to store images. Among them, the QSMC represents the color, and the QSNc represents the coordinate information of pixels in the image [15]. In order to store the color information and position information of the image in the quantum state, Li *et al.* mapped  $m$  different colors and  $n$  coordinate position information into the same number of angle values. The QSMC&QSNc can be given as

$$|I\rangle = \frac{1}{2^n} \sum_{i=0}^{2^n-1} |QSMC_i\rangle \otimes |QSNc_i\rangle, \quad (5)$$

where

$$|QSMC_i\rangle = \cos \phi_i |0\rangle + \sin \phi_i |1\rangle, \quad (6)$$

$$|QSNc_i\rangle = \cos \theta_i |0\rangle + \sin \theta_i |1\rangle. \quad (7)$$

In Eq. (6) and Eq. (7),  $\phi_i, \theta_i \in [0, \frac{\pi}{2}]$ ,  $i = 0, 1, \dots, 2^n - 1$ . In practical application, for example, a  $2 \times 2$  QSMC&QSNc quantum image with its quantum state is presented in FIGURE 3.

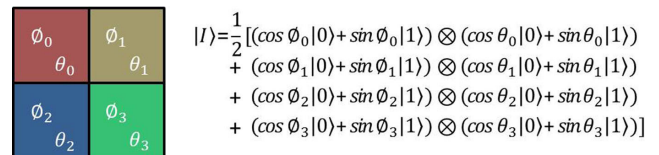


FIGURE 3. A  $2 \times 2$  QSMC&QSNc quantum image and its quantum state (figure adapted from [15]).

QSMC&QSNc can handle image compression and image segmentation well and supports the operation of color image, but it cannot accurately measure the pixel of image.

To reduce the number of identical quantum states used in retrieving an image, Li *et al.* designed algorithm 1 to store an image in a quantum system.

The image of  $N$  pixels are stored in a quantum system with  $2N + m$  qubits by Algorithm 1.

### D. SQR

The SQR stores the pixel information of the infrared image in the quantum state by converting the radiant energy of the object into the quantum state via converter C [16]. Among them, the converter C is a physical device that can detect and record infrared radiant energy and regenerate a quantum state. The SQR can be shown as

$$|I\rangle = |\varphi_{ij}\rangle, \quad (8)$$

**Algorithm 1** Storing an Image in a Quantum System

Step 1: Suppose that  $m$  is the number of different colors of an image, the quantum states of QSMC corresponding to these different colors are stored in a quantum queue  $Q_1$ .

Step 2: Create a bijective function  $F_3 : pos \rightleftharpoons \beta$ , where  $pos = \{1, 2, \dots, m\}$  is a set of the positions in the quantum queue  $Q_1$ , and  $\beta = \{\beta_1, \beta_2, \dots, \beta_m\}$  is an angle set,  $\beta_i = \frac{\pi(i-1)}{2(m-1)}$ ,  $i \in \{1, 2, \dots, m\}$ . If  $m = 1$ , let  $\beta_1 = 0$ . And then,

apply the rotation  $R_y(2\beta_i) = \begin{bmatrix} \cos \beta_i & -\sin \beta_i \\ \sin \beta_i & \cos \beta_i \end{bmatrix}$ , ( $i = 1, 2, \dots, m$ ) on  $|0\rangle$  to create successively  $m$  quantum states.

Step 3: Assume that  $|v_k\rangle$  corresponds to the color of the  $i$ th pixel in the image and is stored in the  $j$ th position of  $Q_1$  which is represented by the quantum state  $|w_j\rangle$ .

Step 4:  $|u_i\rangle$  represents the  $i$ th pixel's coordinate in the image.

Step 5: A quantum composite state  $|\psi_i\rangle = |w_j\rangle \otimes |u_i\rangle$  represents the  $i$ th pixel's color and coordinate.  $|\psi_i\rangle$  is stored in another quantum queue  $Q_2$ .

Step 6: Successively take  $i = 1, 2, \dots, N$ , repeating Step 3 to Step 5 to complete the entire image storage.

where

$$|\varphi_{ij}\rangle = \cos \theta_{ij}|0\rangle + \sin \theta_{ij}|1\rangle. \tag{9}$$

In Eq. (8) and Eq. (9),  $i = 1, 2, \dots, N_1, j = 1, 2, \dots, N_2$ .  $|\varphi_{ij}\rangle$  can store normalized infrared radiant energy collected by the detection unit.  $|I\rangle$  consists of a set of qubits  $|\varphi_{ij}\rangle$ .

In practical application, for example, a  $2 \times 2$  SQR quantum image with its quantum state is shown in FIGURE 4.

$ \varphi_{00}\rangle$	$ \varphi_{01}\rangle$
$ \varphi_{10}\rangle$	$ \varphi_{11}\rangle$

$$|I\rangle = \{|\varphi_{00}\rangle|\varphi_{01}\rangle|\varphi_{10}\rangle|\varphi_{11}\rangle\}$$

$$|\varphi_{00}\rangle = \cos \theta_{00} |0\rangle + \sin \theta_{00} |1\rangle, |\varphi_{01}\rangle = \cos \theta_{01} |0\rangle + \sin \theta_{01} |1\rangle,$$

$$|\varphi_{10}\rangle = \cos \theta_{10} |0\rangle + \sin \theta_{10} |1\rangle, |\varphi_{11}\rangle = \cos \theta_{11} |0\rangle + \sin \theta_{11} |1\rangle.$$

**FIGURE 4.** A  $2 \times 2$  SQR quantum image and its quantum state.

SQR is a kind of infrared quantum image, whose color information is generated by infrared radiation energy, which can improve the visual ability in almost any environment. However, its image retrieval is also probabilistic.

As seen from the representation model of an infrared image,  $N_1 \times N_2$  qubits are needed to store one copy of the normalized infrared image with the size  $N_1 \times N_2$ . The preparation is divided into two steps (See [16]).

**E. QUALPI**

The QUALPI can store and process logarithmic polar coordinate images, which is very helpful for image affine transformation operation [17]. The QUALPI stores the image in a normalized, equally probabilistic superposition state and represents each pixel with the basic state. The QUALPI can

be defined as

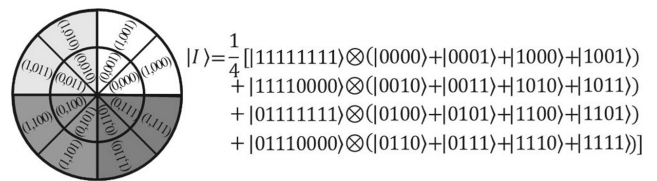
$$|I\rangle = \frac{1}{\sqrt{2^{m+n}}} \sum_{\rho=0}^{2^m-1} \sum_{\theta=0}^{2^n-1} |g(\rho, \theta)\rangle \otimes |\rho\rangle \otimes |\theta\rangle, \tag{10}$$

where  $g(\rho, \theta)$  represents the gray value of the corresponding pixel. When the grayscale range of the image is  $[0, 2^q - 1]$ ,  $g(\rho, \theta)$  can be extended into an equivalent binary sequence, as shown below:

$$g(\rho, \theta) = C_0 C_1 \dots C_{q-2} C_{q-1}, \tag{11}$$

where  $g(\rho, \theta) \in [0, 2^q - 1]$ . It can be seen from Eq. (10) that the basic state of the QUALPI image is composed of tensor products of three quantum sequences, which store the grayscale, polar coordinate radius, and azimuth.

In practical application, for example, a  $2 \times 8$  log - polar quantum image with its quantum state is shown in FIGURE 5.



$$|I\rangle = \frac{1}{4} \{ |11111111\rangle \otimes (|0000\rangle + |0001\rangle + |1000\rangle + |1001\rangle) + |11110000\rangle \otimes (|0010\rangle + |0011\rangle + |1010\rangle + |1011\rangle) + |01111111\rangle \otimes (|0100\rangle + |0101\rangle + |1100\rangle + |1101\rangle) + |01110000\rangle \otimes (|0110\rangle + |0111\rangle + |1110\rangle + |1111\rangle) \}$$

**FIGURE 5.** A  $2 \times 8$  QUALPI quantum image and its quantum state (figure adapted from [17]).

For a  $2^m \times 2^n$  QUALPI image with gray range  $2^q$ , its preparation needs  $m + n + q$  qubits, and the time complexity of the whole quantum image preparation of QUALPI is no more than  $O(q(m + n) \cdot 2^{m+n})$ , which is approximately linear to the resolution of the log-polar image.

QUALPI represents images in logarithmic polar coordinates, so it handles affine transformations very well. Besides, it can provide accurate information retrieval, however, it can only process grayscale images.

**F. NEQR**

The NEQR gives up the method of compiling image color information by angle adopted by the FRQI and uses the basic state of quantum sequence to store color information. The NEQR uses two entangled quantum sequences to store the grayscale information and position information of the image pixels [18]. Assuming that the grayscale range of the image is  $[0, 2^q - 1]$ , for the NEQR image of size  $2^n \times 2^n$ , it can be represented by

$$|I\rangle = \frac{1}{2^n} \sum_{y=0}^{2^n-1} \sum_{x=0}^{2^n-1} |f(y, x)\rangle |yx\rangle = \frac{1}{2^n} \sum_{y=0}^{2^n-1} \sum_{x=0}^{2^n-1} \bigotimes_{i=0}^{q-1} |C_{yx}^i\rangle |yx\rangle, \tag{12}$$

where

$$f(y, x) = C_{yx}^0 \dots C_{yx}^{q-2} C_{yx}^{q-1},$$

$$C_{yx}^k \in [0, 1], \quad \text{and } f(y, x) \in [1, 2^q - 1]. \tag{13}$$

From the representation of NEQR,  $2n+q$  qubits are needed to construct the quantum image model for a  $2^n \times 2^n$  image with gray range  $2^q$ . The whole preparation of NEQR costs no more than  $O(qn2^{2n})$  for a  $2^n \times 2^n$  image with gray range  $2^q$ . This is equivalent to an approximately quadratic decrease compared to FRQI [18].

The preparation process of The NEQR mainly includes two steps: the first step is basically the same as the preparation process of the FRQI; the second step is to set the gray value, which Zhang *et al.* decomposed into  $2^{2n}$  sub-operations and stored the gray information of each pixel one by one [18].

In practical application, for example, a  $2 \times 2$  NEQR quantum image and its quantum state is shown in FIGURE 6.

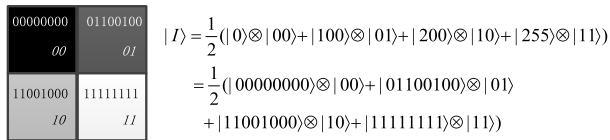


FIGURE 6. A  $2 \times 2$  NEQR quantum image and its quantum state (figure adapted from [18]).

In recent years, relevant researches based on this representation have emerged one after another. Xu, P.G. *et al.* developed a quantum image processing algorithm using the edge extraction method together with the Kirsch operator. In their approach, NEQR is employed as the image representation model for processing quantum images and their proposed algorithm can perform real-time image processing with high accuracy [37].

NEQR uses a normalized quantum superposition state to store grayscale images. For color images, 24 quantum bits are needed to store the color of the image. Also, NEQR can accurately measure the pixel and can be very easy to carry out part of the image transformation.

G. CQIR

The CQIR plays a great role in the realization of histogram equalization of quantum images, and greatly improves many processing algorithms such as negative value calculation, binarization, and color histogram [19], [38]. The CQIR can be represented by

$$|I\rangle = |C\rangle_m \times |P\rangle_{2n} = \frac{1}{2^n} \sum_{i=0}^{2^{2n}-1} \sum_{j=0}^{2^m-1} \alpha_{ij} |j\rangle |i\rangle, \quad (14)$$

where  $0 \leq i \leq 2^{2n}-1$  and  $0 \leq j \leq 2^m-1$ .

In Eq. (14),  $|P\rangle$  is a quantum register composed of  $2n$  qubits, which is used to store pixel position information, while the corresponding color information is stored in  $m$  qubits.  $\alpha_{ij}$  determines the color of the pixel at the position  $i$  through the superposition state of all possible color values.

In practical application, for example, a  $2 \times 2$  CQIR quantum image and its quantum state is shown in FIGURE 7.

CQIR uses a multi-level quantum system to store and process images. It has advantages in terms of the number

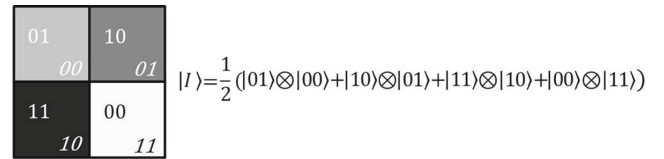


FIGURE 7. A  $2 \times 2$  CQIR quantum image and its quantum state (figure adapted from [19]).

of dimensions of available Hilbert space, computing power, physical implementation and security of quantum cryptographic protocols. However, it can only process grayscale images.

H. MCQI

The MCQI was proposed by Sun *et al.* which can process color images and maintain color information in a normalized state [20]. The MCQI can be shown as

$$|I\rangle = \frac{1}{2^{n+1}} \sum_{i=0}^{2^{2n}-1} |C_{RGB\alpha}^i\rangle \otimes |i\rangle, \quad (15)$$

where  $C_{RGB\alpha}^i$  is used to compile color information. The definition of  $C_{RGB\alpha}^i$  is defined as

$$|C_{RGB\alpha}^i\rangle = \cos \theta_R^i |000\rangle + \cos \theta_G^i |001\rangle + \cos \theta_B^i |010\rangle + \cos \theta_\alpha |011\rangle + \sin \theta_R^i |100\rangle + \sin \theta_G^i |101\rangle + \sin \theta_B^i |110\rangle + \sin \theta_\alpha |111\rangle, \quad (16)$$

where  $\{\theta_R^i, \theta_G^i, \theta_B^i\} \in [0, \pi/2]$ ,  $\theta_R^i, \theta_G^i$  and  $\theta_B^i$  represents the gray value of R, G, and B channels respectively.  $\theta_\alpha$  is usually set to 0.

MCQI can store the RGB information about an image simultaneously by using  $2n + 3$  qubits for encoding  $2^n \times 2^n$  pixel images. In practical application, for example, a  $2 \times 2$  MCQI quantum image with its quantum state is presented in FIGURE 8.

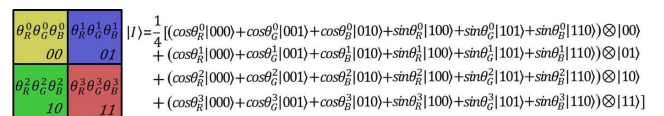


FIGURE 8. A  $2 \times 2$  MCQI quantum image and its quantum state (figure adapted from [20]).

The Polynomial Preparation Theorem (PPT) shows that the MCQI can be constructed using the Hadamard and control rotation gates. The MCQI can realize High-level image processing tasks and use with other processing transformations such as the GTQI, CTQI, and their restricted variants. Besides, the MCQI is used to improve the available image processing tasks such as quantum image watermarking and quantum movie production.

MCQI facilitates more advanced color image processing by performing different operations on the R, G, and B channels of images. Its color information is realized by a controlled phase gate, which makes it very flexible in some image

processing and security algorithms based on phase coding. However, its image retrieval is also based on probability.

### I. INEQR

The NEQR can process the quantum images of size  $2^n \times 2^n$ . However, when the horizontal scaling and the vertical blooming ratio are not equal, the scaled image size is no longer in the form of  $2^n \times 2^n$ . To solve this problem, Jiang and Wang proposed the INEQR [21]. For an INEQR quantum image, it can be expressed as

$$|I\rangle = \frac{1}{2^{\frac{n_1+n_2}{2}}} \sum_{Y=0}^{2^{n_1-1}} \sum_{X=0}^{2^{n_2-1}} |f(Y, X)\rangle |YX\rangle$$

$$= \frac{1}{2^{\frac{n_1+n_2}{2}}} \sum_{Y=0}^{2^{n_1-1}} \sum_{X=0}^{2^{n_2-1}} \bigotimes_{i=0}^{q-1} C_{YX}^i |YX\rangle, \quad (17)$$

where

$$|YX\rangle = |Y\rangle |X\rangle = |y_0 y_1 \dots y_{n_1-1}\rangle |x_0 x_1 \dots x_{n_2-1}\rangle. \quad (18)$$

In Eq. (18),  $y_i, x_i \in \{0, 1\}$ . In the INEQR, Y, X, and F are used to represent the Y-axis, X-axis, and gray values of the image, respectively.

In practical application, for example, a  $2 \times 4$  INEQR quantum image and its quantum state is shown in FIGURE 9.

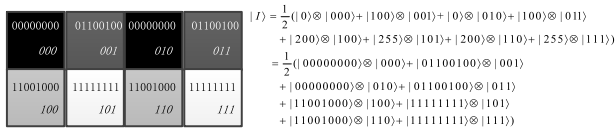


FIGURE 9. A  $2 \times 4$  INEQR quantum image and its quantum state (figure adapted from [21]).

INEQR facilitates image scaling and provides accurate information retrieval.

### J. GNEQR

The GNEQR is a generalized model of the NEQR, which can be represented by

$$|\Psi_{G2}^m\rangle = \frac{1}{\sqrt{2^n}} \sum_{x=0}^{2^{n-k}-1} \sum_{y=0}^{2^k-1} |f(x, y)\rangle |x\rangle |y\rangle \quad (19)$$

where  $|x\rangle = |i_n \dots i_{k+1}\rangle$ ,  $|y\rangle = |i_k \dots i_1\rangle$ , and  $i_1, \dots, i_k, \dots, i_n \in \{0, 1\}$ .  $|x\rangle$  and  $|y\rangle$  represent the X-axis and Y-axis of the graph, respectively.  $f(x, y)$  is the pixel at the coordinate  $(x, y)$  and  $f(x, y) \in C_m$ .  $C_m$  is a color set, which can be shown as

$$C_m = \{0, 1, \dots, 2^m - 1\}. \quad (20)$$

For example, the grayscale color set and RGB color set can be represented as  $C_8 = \{0, 1, \dots, 255\}$  and  $C_{24} = \{0, 1, \dots, 2^{24} - 1\}$ , respectively.

Comparing GNEQR with NEQR, when  $m = q$ , their implementation circuits are the same. In practical application,

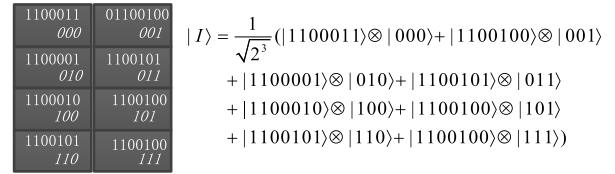


FIGURE 10. A  $4 \times 2$  GNEQR quantum image and its quantum state (figure adapted from [22]).

for example, a  $4 \times 2$  GNEQR quantum image and its quantum state are shown in FIGURE 10.

When  $m$  is 8 or 24,  $|\Psi_{G2}^8\rangle$  and  $|\Psi_{G2}^{24}\rangle$  represent grayscale and color images of  $2^{n-k} \times 2^k$ , respectively. Besides, GNEQR has another color image presentation form. For another representation of RGB color images, we can use  $|\Psi_{GC}^8\rangle$  instead of  $|\Psi_{G2}^8\rangle$  to represent the color image.  $|\Psi_{GC}^8\rangle$  can be defined as

$$|\Psi_{GC}^8\rangle = \frac{1}{\sqrt{3}} \left( |\Psi_{G2r}^8\rangle |01\rangle + |\Psi_{G2g}^8\rangle |10\rangle + |\Psi_{G2b}^8\rangle |11\rangle \right), \quad (21)$$

where  $|\Psi_{G2r}^8\rangle$ ,  $|\Psi_{G2g}^8\rangle$  and  $|\Psi_{G2b}^8\rangle$  represent the Red, Green, or Blue channel of an RGB color image, respectively.  $|\Psi_{G2r}^8\rangle$ ,  $|\Psi_{G2g}^8\rangle$  and  $|\Psi_{G2b}^8\rangle$  are defined as

$$\begin{cases} |\Psi_{G2r}^8\rangle = \frac{1}{\sqrt{2^n}} \sum_{x=0}^{2^{n-k}-1} \sum_{y=0}^{2^k-1} |f_1(x, y)\rangle |x\rangle |y\rangle \\ |\Psi_{G2g}^8\rangle = \frac{1}{\sqrt{2^n}} \sum_{x=0}^{2^{n-k}-1} \sum_{y=0}^{2^k-1} |f_2(x, y)\rangle |x\rangle |y\rangle \\ |\Psi_{G2b}^8\rangle = \frac{1}{\sqrt{2^n}} \sum_{x=0}^{2^{n-k}-1} \sum_{y=0}^{2^k-1} |f_3(x, y)\rangle |x\rangle |y\rangle, \end{cases} \quad (22)$$

where  $f_1(x, y)$ ,  $f_2(x, y)$  and  $f_3(x, y)$  denotes the Red, Green, and Blue channels of the color of the pixel on the coordinate  $(x, y)$ .

For a  $2^{n-k} \times 2^k$  color image,  $|\Psi_{G2}^{24}\rangle$  needs  $(n + 24)$  qubits, but  $|\Psi_{GC}^8\rangle$  uses only  $(n + 10)$  qubits. Therefore,  $|\Psi_{GC}^8\rangle$  is more suitable than  $|\Psi_{G2}^{24}\rangle$  for RGB color images [22].

GNEQR is more versatile than NEQR and is not only suitable for grayscale images, but also for color images. At present, some researchers have carried out relevant researches based on GNEQR. Li *et al.* described the implementation of quantum image operators (e.g. cyclic translation of a quantum image, quantum image translation, and scalar multiplication of a column vector) using elementary quantum arithmetic operations based on GNEQR [39].

### K. NCQI

For a color image, the NCQI uses the base state of the quantum sequence to store the RGB value of each pixel, and all pixels are stored in a normalized superposition state to facilitate simultaneous operation. Inspired by the NEQR,

Sang et al. proposed the NCQI, which can be expressed by

$$|I\rangle = \frac{1}{2^n} \sum_{y=0}^{2^n-1} \sum_{x=0}^{2^n-1} |c(y, x)\rangle \otimes |yx\rangle, \quad (23)$$

where  $c(y, x)$  represents the pixel value at the corresponding coordinate, which can be encoded into a binary sequence  $R_{q-1} \cdots R_0 G_{q-1} \cdots G_0 B_{q-1} \cdots B_0$ , as shown below:

$$|c(y, x)\rangle = |\underbrace{R_{q-1} \cdots R_0}_{\text{Red}} \underbrace{G_{q-1} \cdots G_0}_{\text{Green}} \underbrace{B_{q-1} \cdots B_0}_{\text{Blue}}\rangle. \quad (24)$$

In Eq. (24), the range of values for each channel in the RGB channel is  $[0, 2^q - 1]$ . It takes  $2n + 3q$  qubits to store an NCQI image of size  $2^n \times 2^n$ . In practical application, for example, a  $4 \times 4$  NCQI quantum image and its quantum state is shown in FIGURE 11. It is a  $4 \times 4$  color image with three channels R, G, B ranged  $[0, 2^8 - 1]$ , where  $n = 2$ , and  $q = 8$ .

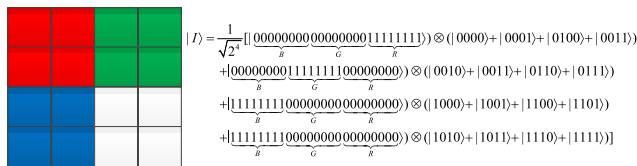


FIGURE 11. A  $4 \times 4$  NCQI quantum image and its quantum state (figure adapted from [23]).

NCQI is more flexible, more suitable for color quantum image processing, and can provide accurate information retrieval.

### L. BRQI

A grayscale image is composed of 8 bitplanes. For grayscale images, each bitplane can be represented by the GNEQR, as shown below:

$$|\Psi_m^j\rangle = \frac{1}{\sqrt{2^n}} \sum_{x=0}^{2^{n-k}-1} \sum_{y=0}^{2^{k-1}} |g(x, y)\rangle |x\rangle |y\rangle, \quad (25)$$

where  $j$  represents the  $j$ -th bitplane,  $j = 0, 1, \dots, 7$ ,  $m = 1$ , and  $g(x, y) \in \mathcal{C}_1 = \{0, 1\}$ . To represent eight bitplanes with one state, the corresponding BRQI is defined as shown in Eq. (25), which contains eight GNEQR states in Eq. (26).

$$\begin{aligned} |\Psi_B^8\rangle &= \frac{1}{\sqrt{2^3}} \sum_{l=0}^{2^3-1} |\Psi_m^l\rangle |l\rangle \\ &= \frac{1}{\sqrt{2^{n+3}}} \sum_{l=0}^{2^3-1} \sum_{x=0}^{2^{n-k}-1} \sum_{y=0}^{2^{k-1}} |g(x, y)\rangle |x\rangle |y\rangle |l\rangle \end{aligned} \quad (26)$$

where  $g(x, y) \in \mathcal{C}_1 = \{0, 1\}$ , and  $l$  represents the  $l$ -th bitplane. It can be seen from the Eq. (26) that the BRQI can represent a grayscale image with only one qubit. Compared to GNEQR, its storage capacity improves 16 times.

An RGB color image can be decomposed into 3 grayscale images or 24 bitplanes. Similar to the Eq. (26), a color image

can be written in three parts, as shown below:

$$\begin{cases} |\Psi_B^R\rangle = \frac{1}{\sqrt{2^{n+3}}} \sum_{l=0}^{2^3-1} \sum_{x=0}^{2^{n-k}-1} \sum_{y=0}^{2^{k-1}} |g_R(x, y)\rangle |x\rangle |y\rangle |l\rangle \\ |\Psi_B^G\rangle = \frac{1}{\sqrt{2^{n+3}}} \sum_{l=0}^{2^3-1} \sum_{x=0}^{2^{n-k}-1} \sum_{y=0}^{2^{k-1}} |g_G(x, y)\rangle |x\rangle |y\rangle |l\rangle \\ |\Psi_B^B\rangle = \frac{1}{\sqrt{2^{n+3}}} \sum_{l=0}^{2^3-1} \sum_{x=0}^{2^{n-k}-1} \sum_{y=0}^{2^{k-1}} |g_B(x, y)\rangle |x\rangle |y\rangle |l\rangle, \end{cases} \quad (27)$$

where  $g_R(x, y), g_G(x, y), g_B(x, y) \in \mathcal{C}_1 = \{0, 1\}$ . The BRQI for RGB images can be defined as

$$|\Psi_B^{24}\rangle = \frac{1}{\sqrt{3}} (|\Psi_B^R\rangle |01\rangle + |\Psi_B^G\rangle |10\rangle + |\Psi_B^B\rangle |11\rangle). \quad (28)$$

Compared with NEQR and NCQI, THE storage capacity of BRQI is increased by 16 times and 218 times respectively, so it has a lower quantum cost. Besides, it can operate on color images.

### M. QRCI

Inspired by the NCQI, Wang et al. proposed the QRCI based on the RGB color model and bitplane [25]. For an RGB image of size  $2^n \times 2^n$ , the color information of the three channels can be compiled as shown below:

$$C_L(Y, X) = R_{LYX} G_{LYX} B_{LYX}, \quad (29)$$

where  $l$  represents the  $l$ -th bitplane,  $R_{LYX}, G_{LYX}, B_{LYX} \in \{0, 1\}$ ,  $L = 0, 1, \dots, 7$ , and  $Y, X = 0, 1, \dots, 2^n - 1$ . The QRCI can be represented by

$$\begin{aligned} |I\rangle &= \frac{1}{\sqrt{2^{2n+3}}} \sum_{L=0}^{2^3-1} \sum_{Y=0}^{2^n-1} \sum_{X=0}^{2^n-1} |C_L(Y, X)\rangle \otimes |LYX\rangle \\ &= \frac{1}{\sqrt{2^{2n+3}}} \sum_{L=0}^{2^3-1} \sum_{Y=0}^{2^n-1} \sum_{X=0}^{2^n-1} |R_{LYX} G_{LYX} B_{LYX}\rangle \otimes |LYX\rangle, \end{aligned} \quad (30)$$

where  $C_L(Y, X)$  represents the color information corresponding to pixel coordinate  $(Y, X)$  on the  $L$ -th bitplane.  $|LYX\rangle$  can be expressed as

$$\begin{aligned} |LYX\rangle &= |L\rangle |Y\rangle |X\rangle \\ &= |L_2 L_1 L_0\rangle |Y_{n-1} Y_{n-2} \dots Y_0\rangle |X_{n-1} X_{n-2} \dots X_0\rangle. \end{aligned} \quad (31)$$

In Eq. (31),  $L$  and  $|YX\rangle$  represent bitplane information and location information, respectively. In practical application, for example, a  $2 \times 2$  QRCI quantum image and its quantum state is shown in FIGURE 12.

Compared with the existing NCQI representation model, the storage capacity of QRCI is improved by 218 times. QRCI can save more storage space than existing quantum image representation models and allow quantum hardware to encrypt any number of images simultaneously. Besides, it can provide accurate information retrieval.

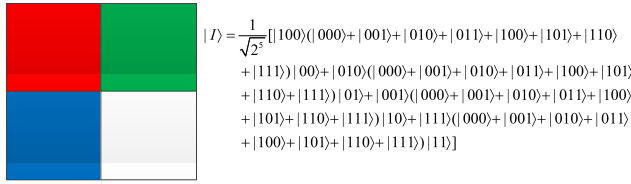


**FIGURE 12.** A 2 × 2 QRCI quantum image and its quantum state (figure adapted from [25]).

**N. QRMMI**

To store multiple images effectively, Zhou *et al.* proposed the QRMMI [26]. Assuming that the digital image with  $T$  the size of  $2^n \times 2^n$  and the image depth  $q$  is represented by the QRMMI, then the color information  $f_J(Y, X)$  at the pixel position  $(Y, X)$  of the  $J$  image can be represented by a binary sequence, as shown below:

$$f_J(Y, X) = C_{JYX}^{q-1} C_{JYX}^{q-2} \dots C_{JYX}^1 C_{JYX}^0, \quad (32)$$

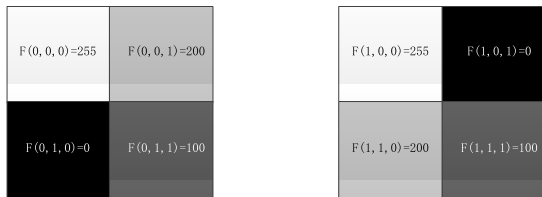
where  $C_{JYX}^k \in \{0, 1\}$ , and  $f_J(Y, X) \in [0, 2^q - 1]$ . In the QRMMI,  $T$  images of size  $A$  can be defined as

$$\begin{aligned} |M\rangle &= \frac{1}{(\sqrt{2})^{2n+t}} \sum_{J=0}^{2^t-1} \sum_{Y=0}^{2^n-1} \sum_{X=0}^{2^n-1} |f_J(Y, X)\rangle \otimes |JYX\rangle \\ &= \frac{1}{(\sqrt{2})^{2n+t}} \sum_{J=0}^{2^t-1} \sum_{Y=0}^{2^n-1} \sum_{X=0}^{2^n-1} |C_{JYX}^{q-1} C_{JYX}^{q-2} \dots C_{JYX}^0\rangle \otimes |JYX\rangle, \end{aligned} \quad (33)$$

where

$$\begin{aligned} |JYX\rangle &= |J\rangle|Y\rangle|X\rangle = |j_{t-1}j_{t-2} \dots j_0\rangle|y_{n-1}y_{n-2} \\ &\dots y_0\rangle|x_{n-1}x_{n-2} \dots x_0\rangle. \end{aligned} \quad (34)$$

In Eq. (34),  $|J\rangle$  and  $|YX\rangle$  represent the serial number and position information of the  $C$ -th image, respectively, and  $t = \lceil \log_2 T \rceil$ . In practical application, for example, two  $2 \times 2$  images represented in the QRMMI and its quantum state is shown as follows.



$$\begin{aligned} |M\rangle &= \frac{1}{(\sqrt{2})^3} (|255\rangle|000\rangle + |200\rangle|001\rangle + |0\rangle|010\rangle + |100\rangle|011\rangle \\ &\quad + |255\rangle|100\rangle + |0\rangle|101\rangle + |200\rangle|110\rangle + |100\rangle|111\rangle) \\ &= \frac{1}{(\sqrt{2})^3} (|11111111\rangle|000\rangle + |11001000\rangle|001\rangle + |00000000\rangle|010\rangle + |01100100\rangle|011\rangle \\ &\quad + |11111111\rangle|100\rangle + |00000000\rangle|101\rangle + |11001000\rangle|110\rangle + |01100100\rangle|111\rangle) \end{aligned}$$

**FIGURE 13.** Two 2 × 2 images represented in the QRMMI and its quantum state (figure adapted from [26]).

In QRMMI, information from multiple images is stored in a specific quantum state. Besides, it can provide accurate information retrieval. However, it only supports operations on grayscale images.

**O. QRMW**

The QRMW is a multi-channel quantum image model of size  $2^n \times 2^m$  [27]. The model uses the base state of the qubit sequence to store the value of different wavelengths of each pixel in the image. The QRMW uses three separate register qubit sequences to store the position, wavelength, and color value of each pixel. It can save the entire image in a superposition of three-qubit sequences. Suppose the number of wavelength channels is  $cn$ , and the maximum color size at any wavelength is  $2^q$ . In the QRMW,  $b$  qubits represent  $cn$  wavelengths,  $q$  qubits represent the color size, and  $n+m$  qubits represent the position information of the image.  $b = \lceil \log_2 cn \rceil$ . The color value of the position  $(y, x)$  in the image channel can be represented by  $f(\lambda, y, x)$ , as shown below:

$$f(\lambda, y, x) = c_{\lambda_{yx}}^0 c_{\lambda_{yx}}^1 \dots c_{\lambda_{yx}}^{q-2} c_{\lambda_{yx}}^{q-1}, \quad (35)$$

where  $\lambda$  and  $yx$  represent channel information and position information, respectively.

A  $2^n \times 2^m$  QRMW image can be written as

$$|I\rangle = \frac{1}{\sqrt{2^{b+n+m}}} \sum_{\lambda=0}^{2^b-1} \sum_{y=0}^{2^n-1} \sum_{x=0}^{2^m-1} |f(\lambda, y, x)\rangle \otimes |\lambda\rangle \otimes |yx\rangle. \quad (36)$$

In practical application, for example, a  $2 \times 2$  QRMW sample image with [0-255] color scale and 4 channels is shown as follows.

$C_0(R) : 11111001$	$C_0(G) : 00001001$
$C_1(G) : 00001011$	$C_1(G) : 11101011$
$C_2(B) : 00011010$	$C_2(B) : 00001010$
$C_3(A) : 11111111$ 00	$C_3(A) : 11111111$ 01
$C_0(R) : 00000001$	$C_0(R) : 11111001$
$C_1(G) : 00001011$	$C_1(G) : 11010101$
$C_2(B) : 11111010$	$C_2(B) : 00001010$
$C_3(A) : 11111111$ 10	$C_3(A) : 11111111$ 11

$$|I\rangle = \frac{1}{4} \left[ \begin{aligned} &|11111001\rangle \otimes |00\rangle \otimes |00\rangle + |00001011\rangle \otimes |01\rangle \otimes |00\rangle + \\ &|00011010\rangle \otimes |10\rangle \otimes |00\rangle + |11111111\rangle \otimes |11\rangle \otimes |00\rangle + \\ &|00001001\rangle \otimes |00\rangle \otimes |01\rangle + |11010101\rangle \otimes |01\rangle \otimes |01\rangle + \\ &|00001010\rangle \otimes |10\rangle \otimes |01\rangle + |11111111\rangle \otimes |11\rangle \otimes |01\rangle + \\ &|00000001\rangle \otimes |00\rangle \otimes |10\rangle + |00001011\rangle \otimes |01\rangle \otimes |10\rangle + \\ &|11111010\rangle \otimes |10\rangle \otimes |10\rangle + |11111111\rangle \otimes |11\rangle \otimes |10\rangle + \\ &|11111001\rangle \otimes |00\rangle \otimes |11\rangle + |11010101\rangle \otimes |01\rangle \otimes |11\rangle + \\ &|00001010\rangle \otimes |10\rangle \otimes |11\rangle + |11111111\rangle \otimes |11\rangle \otimes |11\rangle \end{aligned} \right]$$

**FIGURE 14.** A 2 × 2 QRMW quantum image and its quantum state (figure adapted from [27]).

QRMW has multi-wavelength image representation capability and low time complexity. Besides, it can provide accurate information retrieval. However, it only supports grayscale images.

**P. OCQR**

Liu *et al.* proposed the OCQR based on the NCQI, which uses the 3D quantum sequence to store color quantum images, one



representing the channel value, another representing channel index, and another introducing position information [28]. The OCQR can be expressed as

$$\begin{aligned}
 |I\rangle &= \frac{1}{2^{n+1}} \sum_{y=0}^{2^n-1} \sum_{x=0}^{2^n-1} |c(x, y)\rangle |ch\_index|yx\rangle \\
 &= \frac{1}{2^{n+1}} \sum_{y=0}^{2^n-1} \sum_{x=0}^{2^n-1} \left( |r_{yx}\rangle \otimes |00\rangle + |g_{yx}\rangle \otimes |01\rangle \right. \\
 &\quad \left. + |b_{yx}\rangle \otimes |10\rangle + |s_{yx}\rangle \otimes |11\rangle \right) |yx\rangle,
 \end{aligned} \tag{37}$$

where  $|r_{yx}\rangle = |r_{yx}^{q-1} \dots r_{yx}^0\rangle$ ,  $|g_{yx}\rangle = |g_{yx}^{q-1} \dots g_{yx}^0\rangle$ ,  $|b_{yx}\rangle = |b_{yx}^{q-1} \dots b_{yx}^0\rangle$ , and  $|s_{yx}\rangle = |0^{q-1} \dots 0^0\rangle$ .  $ch\_index$  is the index of the channel, which is usually encoded by two qubits.  $|00\rangle$  represents the red channel index.  $|01\rangle$  represents the green channel index,  $|10\rangle$  represents the blue channel index,  $|11\rangle$  represents the free channel index, which can be used to store other pixel information, such as transparency.

In practical application, for example, a  $2 \times 2$  OCQR quantum image and its quantum state is shown as follows.

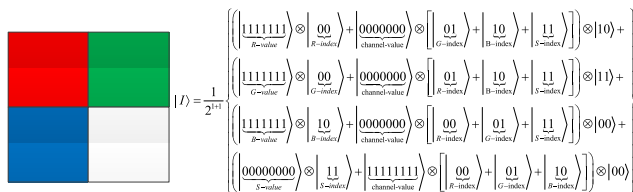


FIGURE 15. A  $2 \times 2$  OCQR quantum image and its quantum state (figure adapted from [28]).

The OCQR takes full advantage of quantum superposition to store the RGB value of each pixel. The OCQR uses nearly a third of the qubits to store pixel values compared to NCQI. At the same time, the OCQR can perform some image processing operations related to color information more conveniently and synchronously. Besides, it also supports color image manipulation.

### Q. FRQCI

To solve the problem of quantum representation of color images, Li and Liu proposed the FRQCI [29]. For a color image of size  $2^n \times 2^n$ , assuming the color range is no more than 255, the RGB color values for the  $k$ -th pixel is  $c_k^R$ ,  $c_k^G$ , and  $c_k^B$ , respectively. The FRQCI can be shown as

$$|I(\theta, \phi)\rangle = \frac{1}{2^n} \sum_{k=0}^{2^{2n}-1} |k\rangle |c_k\rangle, \tag{38}$$

where

$$|c_k\rangle = \cos \frac{\theta_k}{2} |0\rangle + e^{i\phi_k} \sin \frac{\theta_k}{2} |1\rangle, \tag{39}$$

$$\theta_k = \frac{c_k^R \times \pi}{256 - 1}, \tag{40}$$

$$\phi_k = x \frac{(c_k^G \times 256 + c_k^B) \times 2\pi}{256 \times 256 - 1}. \tag{41}$$

In Eq. (41),  $|k\rangle$  is a  $2^{2n}$ -dimensional quantum basis state. The FRQCI state is normalized.

In practical application, for example, a  $2 \times 2$  FRQCI quantum image with its quantum state is presented as follows.

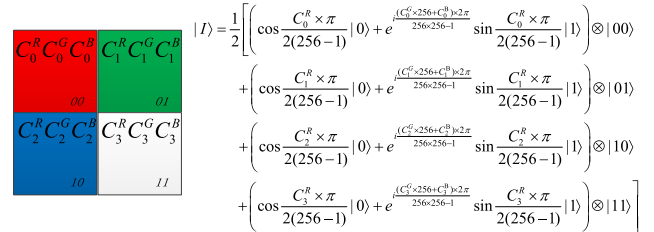


FIGURE 16. A  $2 \times 2$  FRQCI quantum image and its quantum state (figure adapted from [29]).

The FRQCI is an improvement on theFRQI and solves the quantum representation problem of color images.

### R. QMCR

Based on the classical computer RGB model, Abdolmaleky *et al.* extended the grayscale information in the NEQR to the color representation and proposed the QMCR [30]. Two entangled qubit sequences are used to encode the information of the position and color of each pixel. One qubit sequence is used to encode the position of the pixel in the image, and the other qubit sequence is used to encode the red, green, and blue channels' values of the corresponding pixels simultaneously. Assuming that the grayscale range of each color channel is  $2^q$ , a color image of size  $2^n \times 2^n$  using QMCR can be represented by

$$|I\rangle = \frac{1}{2^n} \sum_{y=0}^{2^n-1} \sum_{x=0}^{2^n-1} |C_{RGByx}\rangle \otimes |yx\rangle, \tag{42}$$

where

$$|C_{RGByx}\rangle = |R_{yx}\rangle |G_{yx}\rangle |B_{yx}\rangle, \tag{43}$$

$$|R_{yx}\rangle = |r_{yx}^{q-1} r_{yx}^{q-2} \dots r_{yx}^0\rangle, \tag{44}$$

$$|G_{yx}\rangle = |g_{yx}^{q-1} g_{yx}^{q-2} \dots g_{yx}^0\rangle, \tag{45}$$

$$|B_{yx}\rangle = |b_{yx}^{q-1} b_{yx}^{q-2} \dots b_{yx}^0\rangle. \tag{46}$$

In Eq. (44),

$$r_{yx}^k, g_{yx}^k, b_{yx}^k \in \{0, 1\}, \quad \text{and } R_{yx}, G_{yx}, B_{yx} \in \{0, 1, \dots, 2^q - 1\}.$$

In order to represent the QMCR image,  $3q + 2n$  qubits are needed. In practical application, for example, a  $2 \times 2$  QMCR quantum image and its quantum state is shown as follows.

QMCR is mainly aimed at the application of quantum color images in secure quantum communication, quantum image processing, quantum watermarking, quantum steganography, and quantum data hiding. Besides, it can perform accurate information retrieval.

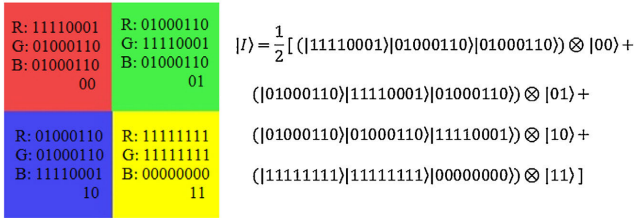


FIGURE 17. A 2 × 2 QMCR quantum image and its quantum state (figure adapted from [30]).

TABLE 1. Proposed method for encoding 2-bit information.

$P_i^{2k+1}P_i^{2k}$	00	01	10	11
$\theta_k$	0	$\frac{\pi}{5}$	$\frac{\pi}{2} - \frac{\pi}{5}$	$\frac{\pi}{2}$

### S. IFRQI

The FRQI uses only one qubit to represent the color information of each pixel. The NEQR uses 2p qubits to represent the intensity of 2p-bit pixels, it does not incorporate the advantage of the superposition principle in this part. Khan proposes the IFRQI which uses p qubits to store the grayscale value of every pixel of a 2p-bit-deep image based on the FRQI and the NEQR [31]. To fully incorporate the advantage of the superposition principle, the IFRQI uses two entangled qubit sequences. The first sequence comprising of p qubits represents the grayscale information of each 2p-bit pixel, while the role of the second qubit sequence is the same as that used in the FRQI model. For an IFRQI image of size  $2^n \times 2^n$  and gray range  $2^{2p}$ , we assume that  $f(i) = P_i^{2p-1}P_i^{2p-2} \dots P_i^1P_i^0$  is the grayscale value of the pixel at the  $i$ th position, where  $P_i^j \in \{0, 1\}$  for all  $j \in \{0, 1, \dots, 2p - 1\}$ . By encoding the 2-bit information  $P_i^{2k+1}P_i^{2k}$  via the angle  $\theta_k$ , we obtain the qubit  $\alpha_{i,k}|0\rangle + \beta_{i,k}|1\rangle$ , where  $\alpha_{i,k} = \cos \theta_k$  and  $\beta_{i,k} = \sin \theta_k$  for all  $0 \leq k \leq p - 1$ .  $\theta_k$  is chosen by the rule given in Table 1. p qubits can be joined together to get  $f(i) = \bigotimes_{k=0}^{p-1} (\alpha_{i,k}|0\rangle + \beta_{i,k}|1\rangle)$ . The IFRQI can be defined as

$$|I_q\rangle = \frac{1}{2^n} \sum_{i=0}^{2^{2n-1}} \bigotimes_{k=0}^{p-1} (\alpha_{i,k}|0\rangle + \beta_{i,k}|1\rangle) \otimes |i\rangle, \quad (47)$$

where  $\alpha_{i,k} = \cos \theta_k$ ,  $\beta_{i,k} = \sin \theta_k$  for all  $0 \leq k \leq p - 1$ .

The quantum image preparation process of IFRQI is given as follows.

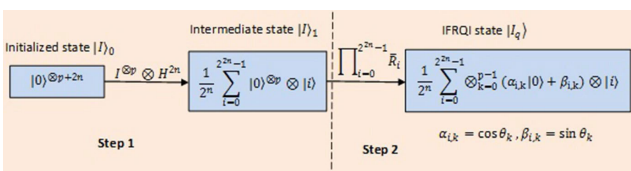


FIGURE 18. Quantum image preparation process of IFRQI model (figure adapted from [31]).

Step 1 is the same as that of the FRQI scheme, and its output is  $|I\rangle_1$ .

$$|I\rangle_1 = \frac{1}{2^n} |0\rangle^{\otimes p} \otimes \sum_{i=0}^{2^{2n-1}} |i\rangle \quad (48)$$

In Step 2, the transformation  $\bar{R}_i$  is defined as follows:

$$\bar{R}_i = \left( I^{\otimes p} \otimes \sum_{j=0, j \neq i}^{2^{2n-1}} |j\rangle\langle j| \right) + L_i \otimes |i\rangle\langle i|, \quad (49)$$

where  $L_i = \bigotimes_{k=0}^{p-1} L_i^k$  and  $L_i^k = R_y(2\theta_k)$ . Here,  $R_y(2\theta_k)$  is a  $2 \times 2$  rotation matrix.  $\bar{R}_i$  acting on  $|I\rangle_1$  can be obtained as follows:

$$\begin{aligned} \bar{R}_i |I\rangle_1 &= \bar{R}_i \left( \frac{1}{2^n} \sum_{j=0}^{2^{2n-1}} |0\rangle^{\otimes p} |j\rangle \right) \\ &= \left( I^{\otimes p} \otimes \sum_{j=0, j \neq i}^{2^{2n-1}} |j\rangle\langle j| + L_i \otimes |i\rangle\langle i| \right) \left( \frac{1}{2^n} \sum_{j=0}^{2^{2n-1}} |0\rangle^{\otimes p} |j\rangle \right) \\ &= \frac{1}{2^n} \left[ \left( I^{\otimes p} \otimes \sum_{j=0, j \neq i}^{2^{2n-1}} |j\rangle\langle j| \right) \left( \sum_{j=0}^{2^{2n-1}} |0\rangle^{\otimes p} |j\rangle \right) \right. \\ &\quad \left. + (L_i \otimes |i\rangle\langle i|) \left( \sum_{j=0}^{2^{2n-1}} |0\rangle^{\otimes p} |j\rangle \right) \right] \\ &= \frac{1}{2^n} \left[ \sum_{j=0, j \neq i}^{2^{2n-1}} |0\rangle^{\otimes p} |j\rangle + L_i |0\rangle^{\otimes p} \otimes |i\rangle \right] \\ &= \frac{1}{2^n} \left[ \sum_{j=0, j \neq i}^{2^{2n-1}} |0\rangle^{\otimes p} |j\rangle + \left( \bigotimes_{k=0}^{p-1} L_i^k \right) (|0\rangle^{\otimes p}) \otimes |i\rangle \right] \\ &= \frac{1}{2^n} \left[ \sum_{j=0, j \neq i}^{2^{2n-1}} |0\rangle^{\otimes p} |j\rangle + \left( \bigotimes_{k=0}^{p-1} (\alpha_{i,k}|0\rangle + \beta_{i,k}|1\rangle) \right) \otimes |i\rangle \right]. \end{aligned} \quad (50)$$

The application of  $U = \prod_{i=0}^{2^{2n-1}-1} \bar{R}_i$  on  $|I\rangle_1$  produces the IFRQI.

The time complexity of the preparation phase of the IFRQI state is  $O(pn2^{2n})$ . To prove this, we need to know the time complexity of the two steps. The complexity of Step 1 is  $O(p + 2n)$ . The complexity of Step 2 is  $O(pn2^{2n})$  [31]. Thus, merge these two steps to get the time complexity of the preparation phase of the IFRQI state.

### T. QBIR

QBIR is proposed for quantum block image representation [32]. Assume the size of the quantum block image  $|I\rangle$  is  $2^w \times 2^w$  and its number is  $2^w \times 2^w$ . Then the QBIR for an

image  $|I\rangle$  can be defined as:

$$\begin{aligned}
 |I\rangle &= \frac{1}{2^n} \frac{1}{2^n} \sum_{j=0}^{2^w-1} \sum_{t=0}^{2^w-1} \sum_{y=0}^{2^{n-w}-1} \sum_{x=0}^{2^{n-w}-1} |C(j, t, y, x)\rangle \otimes |jtx\rangle \\
 &= \frac{1}{2^n} \sum_{j=0}^{2^w-1} \sum_{t=0}^{2^w-1} \sum_{y=0}^{2^{n-w}-1} \sum_{x=0}^{2^{n-w}-1} |c_{jtx}^{q-1} \cdots c_{jtx}^0\rangle |jtx\rangle \otimes |jt\rangle \otimes |yx\rangle,
 \end{aligned} \tag{51}$$

where  $|jtx\rangle$  denotes position information,  $|jt\rangle$  represents the position of blocks and  $|yx\rangle$  represents the position of pixels in each block. In practical application, for example, a  $4 \times 4$  QBIR quantum image and its quantum state is shown as follows.

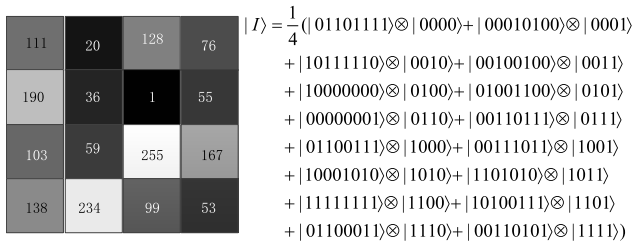


FIGURE 19. A  $4 \times 4$  QBIR quantum image and its quantum state (figure adapted from [32]).

The preparation of QBIR is similar to NEQR, and it includes two steps. In step 1, to store the position information of blocks and pixels, the identity gate

$$\mathbf{I} = \begin{bmatrix} 1 & 0 \\ 0 & 1 \end{bmatrix}$$

and the Hadamard gate

$$\mathbf{H} = \frac{1}{\sqrt{2}} \begin{bmatrix} 1 & 1 \\ 1 & -1 \end{bmatrix}$$

are used to transform the initial quantum state  $|0\rangle^{\otimes 2n+q}$  into a superposition state. Then,  $|M\rangle$  can be got.

$$\begin{aligned}
 |M\rangle &= \mathbf{I}^{\otimes q} \mathbf{H}^{\otimes 2n} (|0\rangle^{\otimes 2n+q}) \\
 &= \frac{1}{2^n} \sum_{j=0}^{2^w-1} \sum_{t=0}^{2^w-1} \sum_{y=0}^{2^{n-w}-1} \sum_{x=0}^{2^{n-w}-1} |0\rangle^{\otimes q} \otimes |jt\rangle \otimes |yx\rangle.
 \end{aligned} \tag{52}$$

In step 2, the  $R_{JTYX}$  is used to set gray information for each pixel  $(Y, X)$  in  $(J, T)$  block.

$$\begin{aligned}
 R_{JTYX} &= \mathbf{I} \otimes \sum_{j=0}^{2^w-1} \sum_{t=0}^{2^w-1} \sum_{y=0}^{2^{n-w}-1} \sum_{x=0, jtx \neq JTYX}^{2^{n-w}-1} |jtx\rangle \langle jtx| \\
 &\quad + \Phi_{JTYX} \otimes |jtx\rangle \langle JTYX|.
 \end{aligned} \tag{53}$$

$\Phi_{JTYX}$  is used to change values of qubits, its definition as follows.

$$\Phi_{JTYX} (|0\rangle^{\otimes q}) = |0\rangle^{\otimes q} \oplus |C(J, T, Y, X)\rangle. \tag{54}$$

By utilizing the operation  $R_{JTYX}$ , we can get

$$\begin{aligned}
 R_{JTYX}(|M\rangle) &= R_{JTYX} \left( \frac{1}{2^n} \sum_{j=0}^{2^w-1} \sum_{t=0}^{2^w-1} \sum_{y=0}^{2^{n-w}-1} |0\rangle^{\otimes q} |jtx\rangle \right) \\
 &= \frac{1}{2^n} \left( \sum_{j=0}^{2^w-1} \sum_{t=0}^{2^w-1} \sum_{y=0}^{2^{n-w}-1} \sum_{x=0, jtx \neq JTYX}^{2^{n-w}-1} |0\rangle^{\otimes q} |jtx\rangle \right. \\
 &\quad \left. + (|0\rangle^{\otimes q} \oplus |C(J, T, Y, X)\rangle) |JTYX\rangle \right) \\
 &= \frac{1}{2^n} \left( \sum_{j=0}^{2^w-1} \sum_{t=0}^{2^w-1} \sum_{y=0}^{2^{n-w}-1} \sum_{x=0, jtx \neq JTYX}^{2^{n-w}-1} |0\rangle^{\otimes q} |jtx\rangle \right. \\
 &\quad \left. + |C(J, T, Y, X)\rangle |JTYX\rangle \right).
 \end{aligned} \tag{55}$$

A total of  $2^{2n}$  operations of  $R_{JTYX}(|M\rangle)$  are needed to prepare an image. The operation is defined as follows.

$$\begin{aligned}
 &\prod_{j=0}^{2^w-1} \prod_{t=0}^{2^w-1} \prod_{y=0}^{2^{n-w}-1} \prod_{x=0}^{2^{n-w}-1} R_{JTX}(|M\rangle) \\
 &= \frac{1}{2^n} \sum_{j=0}^{2^w-1} \sum_{t=0}^{2^w-1} \sum_{y=0}^{2^{n-w}-1} \sum_{x=0}^{2^{n-w}-1} \Phi_{JTYX} (|0\rangle^{\otimes q}) \otimes |jt\rangle \otimes |yx\rangle \\
 &= \frac{1}{2^n} \sum_{j=0}^{2^w-1} \sum_{t=0}^{2^w-1} \sum_{y=0}^{2^{n-w}-1} \sum_{x=0}^{2^{n-w}-1} |C(J, T, Y, X)\rangle |JTYX\rangle.
 \end{aligned} \tag{56}$$

Through the above two steps, the preparation of QBIR is completed.

### U. OQIM

OQIM uses the basis state of a qubit sequence to store the ascending order of each pixel according to their gray values' magnitude. OQIM quantum image model is more flexible and better suited for histogram specification, histogram equalization, and other similar image enhancement method such as luminance correction and so on than the existing models [33]. The OQIM can be expressed as

$$|I\rangle = \frac{1}{2^{n+1/2}} \sum_{i=0}^{2^{2n}-1} |cp_i\rangle \otimes |i\rangle, \tag{57}$$

where  $|cp_i\rangle = \cos \theta_i |00\rangle + \sin \theta_i |10\rangle + \cos \varphi_i |01\rangle + \sin \varphi_i |11\rangle$ ,  $|i\rangle$  encodes the sorted position with the basis state of a qubit sequence from  $|00 \cdots 00\rangle$  to  $|11 \cdots 11\rangle$ .  $\cos \theta_i |00\rangle + \sin \theta_i |10\rangle$  represents the color quantum state of image in pixel  $i$ , and  $\cos \varphi_i |01\rangle + \sin \varphi_i |11\rangle$  represents the  $i$ th coordinate quantum state according to the real coordinate position in the image with  $\varphi = (\varphi_0, \varphi_1, \dots, \varphi_{2^{2n}-1})$  being the angle vector. The gray value  $\theta_i$  is mapped to  $[0, \pi/2]$  from the scope  $[0, L]$ ,  $L$  is the max gray level, and  $\theta = (\theta_0, \theta_1, \dots, \theta_{2^{2n}-1})$  is the angle vector with  $\theta_i \in [0, \pi/2]$ .  $\varphi_i$  is mapped to  $[0, \pi/2]$  from the scope  $[0, 2^{2n}-1]$ .  $|p\rangle$  control the distinguishability between the color and the coordinate position. When  $|p\rangle = |1\rangle$  or  $|p\rangle = |0\rangle$ ,  $|cp_i\rangle$  represent the coordinates or the colors. For an OQIM quantum image of size  $2^n \times 2^n$ , we need  $2n + 2$  qubits

$\Theta_3 \varphi_3$	$\Theta_0 \varphi_0$
$11$	$00$
$\Theta_2 \varphi_2$	$\Theta_1 \varphi_1$
$10$	$01$

$$|I\rangle = \frac{1}{2^{3/2}} [(\cos \theta_0 |00\rangle + \sin \theta_0 |10\rangle + \cos \varphi_0 |01\rangle + \sin \varphi_0 |11\rangle) \otimes |00\rangle + (\cos \theta_1 |00\rangle + \sin \theta_1 |10\rangle + \cos \varphi_1 |01\rangle + \sin \varphi_1 |11\rangle) \otimes |01\rangle + (\cos \theta_2 |00\rangle + \sin \theta_2 |10\rangle + \cos \varphi_2 |01\rangle + \sin \varphi_2 |11\rangle) \otimes |10\rangle + (\cos \theta_3 |00\rangle + \sin \theta_3 |10\rangle + \cos \varphi_3 |01\rangle + \sin \varphi_3 |11\rangle) \otimes |11\rangle]$$

**FIGURE 20. A 2 × 2 OQIM quantum image and its quantum state (figure adapted from [33]).**

to store it. In practical application, for example, a 2 × 2 OQIM quantum image and its quantum state are shown as follows.

In the preparation for OQIM, firstly, 2n + 2 qubits are initialized by the equation  $|I\rangle_{in} = |0\rangle^{\otimes 2n+2}$ . Then,  $|I\rangle_{in}$  become the middle state  $|I\rangle_{mi}$  by using the quantum operator  $U_1 = I \otimes H^{\otimes 2n+1}$ .

$$\begin{aligned} |I\rangle_{mi} &= U_1 (|I\rangle_{in}) = I \otimes H^{\otimes 2n+1} (|0\rangle^{\otimes 2n+2}) \\ &= I(|0\rangle) \otimes H(|0\rangle) \otimes H^{\otimes 2n} (|0\rangle^{\otimes 2n}) \\ &= \frac{1}{2^{n+1/2}} |0\rangle \otimes \sum_{l=0}^1 |l\rangle \otimes \sum_{i=0}^{2^n-1} |i\rangle. \end{aligned} \quad (58)$$

Now, every sorted position is stored into a normalized quantum superposition state. Then, we perform the next quantum transformation to assign the color values and coordinates to these sorted positions by the superposed  $2^{2n}$  quantum states.  $R_y(2\theta)$  and  $R_y(2\varphi)$  are rotation matrices (the rotations about Y axis by the angle  $2\theta$  and  $2\varphi$ , respectively).

$$\begin{aligned} R_y(2\theta) &= \begin{bmatrix} \cos \theta & -\sin \theta \\ \sin \theta & \cos \theta \end{bmatrix} \\ R_y(2\varphi) &= \begin{bmatrix} \cos \varphi & -\sin \varphi \\ \sin \varphi & \cos \varphi \end{bmatrix}. \end{aligned} \quad (59)$$

Then, we construct two control rotation matrices for the color values and coordinates, respectively,

$$\begin{aligned} R_{c,i} &= R_y(2\theta_i) \otimes (|0\rangle\langle 0|) \\ R_{p,i} &= R_y(2\varphi_i) \otimes (|1\rangle\langle 1|). \end{aligned} \quad (60)$$

Then, we can obtain  $R_i = R_{c,i}R_{p,i}$  and  $R_{cp,i}$ .

$$R_{cp,i} = \left( I^{\otimes 2} \otimes \sum_{j=0, j \neq i}^{2^n-1} |j\rangle\langle j| \right) + R_i \otimes |i\rangle\langle i|. \quad (61)$$

Here,  $R_{cp,i}$  is a unitary matrix. Let  $i = k$ , using  $R_{cp,i}$  on  $|I\rangle_{mi}$ , we can obtain

$$\begin{aligned} R_{cp,k} (|I\rangle_{mi}) &= R_{cp,k} \left( \frac{1}{2^{n+1/2}} |0\rangle \otimes \sum_{l=0}^1 |l\rangle \otimes \sum_{i=0}^{2^n-1} |i\rangle \right) \\ &= \left( I^{\otimes 2} \otimes \sum_{j=0, j \neq k}^{2^n-1} |j\rangle\langle j| + R_k \otimes |k\rangle\langle k| \right) \\ &\cdot \left( \frac{1}{2^{n+1/2}} |0\rangle \otimes \sum_{l=0}^1 |l\rangle \otimes \sum_{i=0}^{2^n-1} |i\rangle \right) \end{aligned}$$

$$= \frac{1}{2^{n+1/2}} \begin{pmatrix} (\cos \theta_k |00\rangle + \sin \theta_k |10\rangle + \cos \varphi_k |01\rangle + \sin \varphi_k |11\rangle) \\ \otimes |k\rangle + |0\rangle \otimes \sum_{l=0}^1 |l\rangle \otimes \sum_{i=0, i \neq k}^{2^n-1} |i\rangle \end{pmatrix}. \quad (62)$$

Then, let  $R_{cp} = R_{cp,0}R_{cp,1} \cdots R_{cp,2^n-1}$  and perform  $R_{cp}$  on  $|I\rangle_{mi}$ , we can obtain the final preparation of OQIM.

$$\begin{aligned} R_{cp} (|I\rangle_{mi}) &= R_{cp} \left( \frac{1}{2^{n+1/2}} |0\rangle \otimes \sum_{l=0}^1 |l\rangle \otimes \sum_{i=0}^{2^n-1} |i\rangle \right) \\ &= \frac{1}{2^{n+1/2}} \sum_{i=0}^{2^n-1} \begin{pmatrix} \cos \theta_i |00\rangle + \sin \theta_i |10\rangle \\ + \cos \varphi_i |01\rangle + \sin \varphi_i |11\rangle \end{pmatrix} \\ &\otimes |i\rangle. \end{aligned} \quad (63)$$

Besides, we can find that the complexity of this preparation of OQIM is  $O(2^{4n})$ .

### V. QIIR

Based on the classical representation of indexed images, QIIR uses two quantum data structures  $|Q_{Data}\rangle$  and  $|Q_{Map}\rangle$  to represent quantum data matrix and quantum palette matrix respectively, each data structure uses the basic states of qubit sequence to store information. For an indexed image with the size  $2^n \times 2^n$  and the bit depth  $q$ ,  $|Q_{Data}\rangle$  can be expressed as:

$$|Q_{Data}\rangle = \frac{1}{2^n} \sum_{Y=0}^{2^n-1} \sum_{X=0}^{2^n-1} |I_{YX}\rangle \otimes |YX\rangle \quad (64)$$

where  $|YX\rangle = |Y_{n-1}Y_{n-2} \cdots Y_0 X_{n-1}X_{n-2} \cdots X_0\rangle$  is the 2-dimensional position coordinate of each pixel,  $\{Y_i\}_{i=0}^{n-1} \in \{0, 1\}$ ,  $\{X_i\}_{i=0}^{n-1} \in \{0, 1\}$ ;  $|I_{YX}\rangle = |I_{YX}^{q-1} I_{YX}^{q-2} \cdots I_{YX}^1 I_{YX}^0\rangle$  is the pixel value, which is also the index into the palette matrix,  $\{I_{YX}^i\}_{i=0}^{q-1} \in \{0, 1\}$ . For an indexed image with the bit depth  $q$ ,  $|Q_{Map}\rangle$  can be expressed as:

$$|Q_{Map}\rangle = \frac{1}{\sqrt{2^q}} \sum_{j=0}^{2^q-1} |C_j\rangle \otimes |j\rangle \quad (65)$$

where  $|j\rangle = |j_{q-1}j_{q-2} \cdots j_0\rangle$  is the index in the palette matrix,  $\{j_i\}_{i=0}^{q-1} \in \{0, 1\}$ ;  $|C_j\rangle = |C_j^{23} C_j^{22} \cdots C_j^0\rangle$ ,  $\{|C_j^i\}_{i=16}^{23}$ ,  $\{|C_j^i\}_{i=8}^{15}$ ,  $\{|C_j^i\}_{i=10}^7$  are respectively the red, green and blue component values in a single color,  $\{C_j^i\}_{i=0}^{23} \in \{0, 1\}$ . A simple example of an indexed image is shown as follows.

The representation models of a quantum data matrix  $|Q_{Data}\rangle$  and a quantum palette matrix  $|Q_{Map}\rangle$  are similar to NEQR. For an image with the size  $2^n \times 2^n$ , the color range  $2^c$ , the bit depth  $q$ , the time complexity of  $|Q_{Data}\rangle$ ,  $|Q_{Map}\rangle$ ,  $|Q_{Data}\rangle + |Q_{Map}\rangle$  are  $O(qn \cdot 2^{2n})$ ,  $O(2^q \cdot \frac{c}{2})$ ,  $O(qn \cdot 2^{2n} + 2^q \cdot \frac{c}{2})$ , respectively. The number of used qubits of  $|Q_{Data}\rangle$ ,  $|Q_{Map}\rangle$ ,  $|Q_{Data}\rangle + |Q_{Map}\rangle$  are  $2n + q$ ,  $q + c$ ,  $2n + 2q + c$ , respectively.

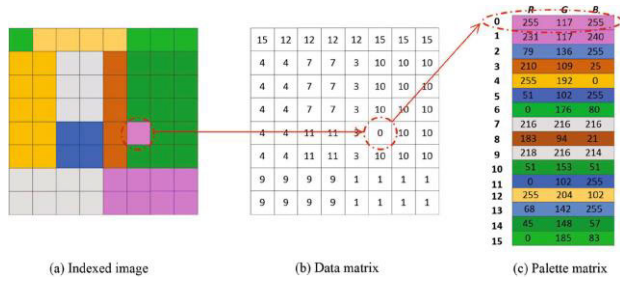


**FIGURE 21.** A simple example of indexed image (figure adapted from [8]).

**W. DQRCI**

Based on QRCI, Wang *et al.* proposed DQRCI which can store two color digital images simultaneously into a quantum superposition state is investigated [34]. The DRQCI can be shown as

$$\begin{aligned}
 |D\rangle &= \frac{1}{\sqrt{2^{2n+3}}} \sum_{L=0}^{2^3-1} \sum_{Y=0}^{2^n-1} \sum_{X=0}^{2^n-1} |C(L, Y, X)\rangle \otimes |L\rangle \otimes |YX\rangle \\
 &= \frac{1}{\sqrt{2^{2n+3}}} \sum_{L=0}^{2^3-1} \sum_{Y=0}^{2^n-1} \sum_{X=0}^{2^n-1} |C_L^1(Y, X)C_L^2(Y, X)\rangle \\
 &\quad \otimes |L\rangle \otimes |YX\rangle \\
 &= \frac{1}{\sqrt{2^{2n+3}}} \sum_{L=0}^{2^3-1} \sum_{Y=0}^{2^n-1} \sum_{X=0}^{2^n-1} |R_{LYX}^1 G_{LYX}^1 B_{LYX}^1 R_{LYX}^2 G_{LYX}^2 B_{LYX}^2\rangle \\
 &\quad \otimes |L\rangle \otimes |YX\rangle \tag{66}
 \end{aligned}$$

where  $|C_L^1(Y, X)\rangle = |R_{LYX}^1 G_{LYX}^1 B_{LYX}^1\rangle$  and  $|C_L^2(Y, X)\rangle = |R_{LYX}^2 G_{LYX}^2 B_{LYX}^2\rangle$  represent the color information of pixel  $|YX\rangle$  in bit-plane  $|L\rangle$  in two images, respectively. DQRCI only employs  $2n + 9$  qubits to store two color digital images of size  $2^n \times 2^n$  with every channel ranged  $[0, 255]$ . In practical application, for example, two  $2 \times 2$  color images represented in the DQRCI and its quantum state is shown as follows.

**X. SUMMARY OF QUANTUM IMAGE REPRESENTATIONS**

In this section, the quantum image representations introduced above are analyzed and summarized. We summarized from the formula of quantum image representation, the coding method of color position information, the computational complexity of image preparation, and measurement retrieval of quantum image.

Most of the recent quantum image representations are focused on modifying the three pioneering quantum image representations. In Table 2, we can get that FRQI, QUALPI NEQR, CQIR INEQR, QRMMI, QRMW, OQIM can only deal with the gray image. NAQSS, QSMC&QSNC MCQI, GNEQR NCQI, BRQI, OCQR, QMCR, IFRQI, QIIR, DQRCI can operate on color images. Besides, SQR is a representation of infrared quantum images where the color information is produced from infrared radiation energy that could improve the visual capacity in almost any environment. QUALPI, NEQR CQIR, INEQR GNEQR, NCQI, BRQI,

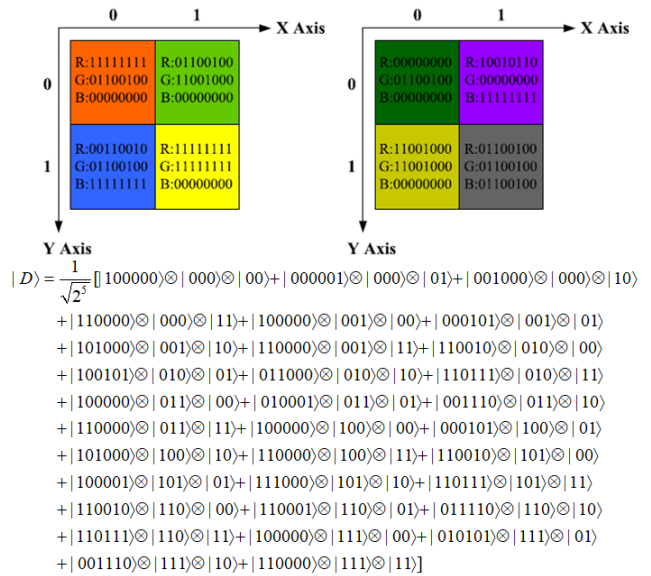


**FIGURE 22.** Two color digital images with size  $2 \times 2$  and its DQRCI quantum state (figure adapted from [34]).

QRCI, QRMMI, QRMW, OCQR, QMCR, QBIR, QIIR, DQRCI can provide more accurate information retrieval.

For an image with the same size, i.e.  $2^n \times 2^n$ , required qubits for different quantum image representations are discussed in Table 3.

On the comparison of quantum image expressions, Li *et al.* discuss the storage and retrieval technologies of quantum images by using some typical examples of QIRs of three categories and compared them in their book [40].

FRQI has the advantage of a quantum superposition state, where the quantum state of the stored image is normalized. Also, FRQI is suitable for full image transformation, which is fast, but not for partial image transformation, FRQI cannot perform accurate image measurements and is limited to grayscale images. NAQSS can satisfy multi-dimensional color image processing and improve the efficiency and accuracy of image segmentation. However, it cannot precisely measure the pixels of an image. QSMC&QSNC can handle image compression and image segmentation very well. it cannot precisely measure the pixels of an image. SQR is a representation of infrared quantum images where the color information (a quantum state) is produced from infrared radiation energy that could improve the visual capacity in almost any environment. Similarly, its image retrieval is based on probabilistic. QUALPI represents the image in logarithmic polar coordinates, so it handles affine transformations very well. Besides, it can provide accurate information retrieval. NEQR uses a normalized quantum superposition state to store grayscale images, and for color images, 24 quantum bits are required to store the color of an image. Also, NEQR can accurately measure the pixel and can be very convenient to do part of the image transformation. CQIR uses multilevel quantum systems to store and process images. It has advantages in terms of dimension of the available Hilbert space,

TABLE 2. Comparison of different quantum image representations.

QIR	Equation	Color encoding	Position encoding	Complexity	Retrieval
FRQI	Eqs. (1)	1 angle vector -> grayscale /RGB	1 2n-D quantum sequence	$O(2^{4n})$	Probabilistic
NAQSS	Eqs. (3)	1 angle vector -> grayscale /RGB	n+1 qubits	$O(\log 2^n \cdot 2^{2n})$	Probabilistic
QSMC&QSNC	Eqs. (5)	1 angle vector -> grayscale /RGB	1 angle vector	$O(2^{4n})$	Probabilistic
SQR	Eqs. (8)	1 angle vector -> infrared quantum sequence	1 quantum sequence	$O(2^{2n})$	Probabilistic
QUALPI	Eqs. (10)	grayscale quantum sequence -> grayscale quantum sequence	2 quantum sequence	$O(q(m+n) \cdot 2^{mn})$	Deterministic
NEQR	Eqs. (12)	grayscale quantum sequence -> grayscale quantum sequence	1 quantum sequence	$O(qn \cdot 2^{2n})$	Deterministic
CQIR	Eqs. (14)	grayscale quantum sequence -> grayscale quantum sequence	1 quantum sequence	$O(\log_2 L \cdot n \cdot 2^{2n})$	Deterministic
MCQI	Eqs. (15)	grayscale 3 angle vector -> RGB quantum sequence	1 quantum sequence	$O(2^{4n})$	Probabilistic
INEQR	Eqs. (17)	grayscale quantum sequence -> grayscale quantum sequence	2 quantum sequence	$O(q(n_1+n_2) \cdot 2^{n_1 n_2})$	Deterministic
GNEQR	Eqs. (19)	grayscale quantum sequence -> grayscale /RGB quantum sequence	2 quantum sequence	$O(mn \cdot 2^n)$	Deterministic
NCQI	Eqs. (23)	grayscale quantum sequence -> RGB quantum sequence	1 quantum sequence	$O(3q+2n+6qn \cdot 2^{3n})$	Deterministic
BRQI	Eqs. (26)	grayscale quantum sequence -> grayscale /RGB quantum sequence	3 quantum sequence	$O(mn \cdot 2^n)$	Deterministic
QRCI	Eqs. (30)	grayscale quantum sequence -> RGB quantum sequence	3 quantum sequence	$O(L \cdot 2^{2n})$	Deterministic
QRMMI	Eqs. (33)	grayscale quantum sequence -> grayscale quantum sequence	3 quantum sequence	$O(n2^{3n})$	Deterministic
QRMW	Eqs. (36)	grayscale quantum sequence -> grayscale quantum sequence	1 quantum sequence	$O(q \cdot 2^{4n})$	Deterministic
OCQR	Eqs. (37)	grayscale quantum sequence -> RGB quantum sequence	1 quantum sequence	$O(3q(2n+2)2^{2n})$	Deterministic
FRQCI	Eqs. (38)	3 angle vector -> RGB quantum sequence	1 quantum sequence	$O(2^{4n})$	Probabilistic
QMCR	Eqs. (42)	Quantum sequence -> RGB quantum sequence	1 quantum sequence	$O(qn \cdot 2^{4n})$	Deterministic
IFRQI	Eqs. (47)	Quantum sequence -> RGB quantum sequence	1 quantum sequence	$O(pn2^{2n})$	Probabilistic
QBIR	Eqs. (51)	Quantum sequence -> block	1 quantum sequence	$O(qn \cdot 2^{2n})$	Deterministic

computational power, physical implementation, and security of quantum cryptographic protocols. MCQI facilitates more advanced color image processing by applying different

TABLE 2. (Continued) Comparison of different quantum image representations.

OQIM	Eqs. (57)	image 1 angle vector -> grayscale	1 quantum sequence	$O(2^{4n})$	Probabilistic
QIIR	Eqs. (64), (65)	Quantum sequence -> RGB quantum sequence	1 quantum sequence	$O(qn \cdot 2^{2n} + 2^n \frac{q}{2})$	Deterministic
DQRCI	Eqs. (66)	Quantum sequence -> RGB quantum sequence	3 quantum sequence	$O(L \cdot 2^{2n})$	Deterministic

TABLE 3. Comparison of required qubits for different quantum image representations of size  $2^n \times 2^n$ .

QIR	Required qubits	QIR	Required qubits
FRQI	$2n+1$	GNEQR	$n+8 [G]/ n+10 [C]$
NAQSS	$2n+1$	NCQI	$2n+3q$
QSMC&QSNC	$4n$	BRQI	$n+3 [G]/ 3n+9 [C]$
SQR	$2n$	QRCI	$2n+3$
QUALPI	$2n+q$	QRMMI	$2n+t+q$
NEQR		QRMW	$2n+b+q$
CQIR	$2n+m$	OCQR	$2n+4q$
MCQI	$2n+3$	FRQCI	$6n$
INEQR	$2n+8 [G]/ 2n+10 [C]$	QMCR	$2n+3q$
IFRQI	$2n+p$	QBIR	$2n$
OQIM	$2n+2$	QIIR	$2n+2q+c$
DQRCI	$2n+9$	-	-

Note: "G" represents grayscale image, "C" represents color image.

operations on the R, G, and B channels of the image. INEQR is convenient for image scaling operations. GNEQR is more versatile than NEQR and is not only suitable for grayscale images, but also for color images. Many color operations can be executed conveniently based on NCQI. The NCQI is more flexible and better suited to carry out color quantum image processing. Compared with NEQR and NCQI, The storage capacity of BRQI is improved by 16 times and 218 times respectively, so it has a lower quantum cost. Compared with the existing NCQI representation model, the storage capacity of QRCI improves  $2^{18}$  times. QRCI could save more storage space than the existing quantum image representation models and allow quantum hardware to encrypt an arbitrary number of images simultaneously. In the QRMMI, the information of multiple images is stored in a specific quantum state. QRMW is capable of multi-wavelength image representation and has less time complexity. OCQR makes full use of quantum superposition characteristic to store the RGB value of every pixel. Compared with NCQI, OCQR uses nearly one-third times the qubits to store the pixel value. Meanwhile, some image processing operations related to color information can be executed more simultaneously and conveniently based on OCQR. FRQCI improves on FRQI by solving the problem of quantum representation of color images. QMCR is mainly proposed for the applications of quantum color images in secure quantum communication, quantum image

processing, quantum watermarking, quantum steganography, and quantum data hiding and so on. The time complexity of image preparation in FRQI model is lower than that in NEQR model. The IFRQI model is comparable to FRQI and NEQR models through the performance analysis in respect of time and space complexity. QBIR can manipulate quantum image blocks flexibly. OQIM quantum image model is more flexible and better suited for histogram specification, histogram equalization and other similar image enhancement method such as luminance correction and so on than the existing models. QIIR can solve the representation problem of indexed images on a quantum computer. DQRCI can store two color digital images simultaneously into a quantum superposition state.

### III. OPEN CHALLENGES AND FUTURE RESEARCH DIRECTIONS

Quantum image processing is a multi-disciplinary comprehensive field, which is currently in its infancy. The research mainly focuses on the development of processing tools, and there are still interdisciplinary studies to be explored [41], [33]. It is a field full of exciting open problems for many researchers [1].

#### A. ALGORITHM RESEARCH

In classical image processing, the related processing algorithms mainly include image color processing, image geometric position processing, image morphology, image segmentation, object recognition, image recovery, image compression, image encryption, and so on. However, in the field of quantum image processing, there are too few corresponding image processing algorithms, so researchers need to do a lot of work [42]–[54].

In terms of classical information and quantum information, with the development of quantum computing, some algorithms that are difficult to solve are expected to be solved in the future. Currently, there are many research results on classical image processing in quantum mechanical systems, but few that address the physical storage, processing, and visualization of quantum information. Therefore, we also need to design specialized quantum processing algorithms for the signals and images generated by quantum information sources. In addition, for data visualization, quantum image processing techniques can be used to process and visualize data emitted by devices such as quantum light sources [55]. In the field of science and engineering, the main directions of development are in basic scientific research, applied engineering and the military field. In basic science research, quantum image processing algorithms can be used to visualize experimental results, such as optimization super-resolution algorithms [56]. In terms of application engineering, the quantum image processing algorithm can be applied in medical imaging, automatic monitoring, pattern recognition, nano manufacturing, and other fields [57]–[59]. In terms of the military, image processing is an important part of this, while quantum

computing and quantum information are also areas of interest for military applications, such as quantum radar [60]–[63].

#### B. RESEARCH ON THE METHOD OF QIP ADVANTAGE DISPLAY

In general, we measure the advantages of quantum image processing algorithms by comparing their time complexity with traditional image processing algorithms, but this is often not enough. It is more appropriate to explore an accurate and comprehensive way to show the advantages of QIP and to make a comprehensive comparison between the process and result [64]–[67]. In the future, quantum image processing algorithms are used to develop quantum algorithms related to areas such as computer vision, automatic detection, and manufacturing, resulting in a range of basic or advanced image processing algorithms. In addition to the increase in computational speed in the theoretical sense, quantum computing also has the realistic possibility of playing a role in different fields. In the current era of big data and artificial intelligence, quantum computing can solve the problem of massive data retrieval, as well as the current overwhelming problem of logistics optimization, cost savings and carbon emission reduction. In the era of massive and complex information, powerful data analysis and sorting tools are undoubtedly of great help to people's lives and work. In quantum simulation, particularly in biopharmaceuticals, quantum simulation promises to accurately simulate molecules over longer time scales using corresponding quantum algorithms. This will help accelerate the search for new, life-saving drugs and significantly shorten the drug development cycle by enabling accurate modeling that is not possible with current technology. In finance, quantum computing impacts the financial services industry by addressing complex optimization problems such as portfolio risk optimization and fraud detection. Quantum computing allows for better identification of attractive portfolios with thousands of assets with interconnected dependencies, and for more effective identification of key fraud patterns. In artificial intelligence, quantum computing can effectively improve the depth and speed of machine learning and break through the bottleneck of AI development. Quantum machine learning can help AI perform complex tasks more effectively in a human-like manner, for example, enabling humanoid robots to make optimal decisions in real-time in unpredictable situations. Training AI on a quantum computer can improve the performance of computer vision recognition, pattern recognition, speech recognition, machine translation, and more. In modern agriculture, quantum computers can make fertilizer more efficiently. Nearly all fertilizers are made from ammonia, and increasing the ability to produce ammonia (or alternatives) means cheaper, less energy-intensive fertilizers; high-quality fertilizers would be good for the environment and help feed the planet's growing population; but because the number of catalyst combinations is infinite, little progress has been made in improving the process of making or replacing ammonia. It would take centuries to digitally test today's supercomputers to find the

right combination of catalysts to make ammonia; however, quantum computers can quickly analyze chemical catalysis processes and come up with the best combination of catalysts to produce ammonia. Besides, quantum cloud computing is becoming a promising field. Quantum cloud platforms can simplify programming and provide low-cost access to quantum computers, and major companies, including IBM, Google, and Alibaba, are deploying quantum cloud computing projects. Quantum computers can be used to crack the codes that protect the security of sensitive data and electronic communications, and they can also be used to protect data from quantum hacking, which requires a technique known as quantum encryption. Quantum encryption is the idea of transmitting entangled photons over long distances via quantum key distribution to protect sensitive communications; most importantly, if a quantum encrypted communication is intercepted, the encryption scheme will immediately show signs of disruption and indicate that the communication is not secure. This relies on the principle that measuring the behavior of a quantum system can destroy the system, known as the “measurement effect”. As the cost of quantum computing resources decreases and quantum fundamentals become more widely available, more relevant industry players will emerge, and quantum computing will be increasingly used in a variety of industries, especially in areas where traditional computers are inefficient.

### C. PHYSICAL EXPERIMENTAL RESEARCH

At present, all quantum image processing schemes stay in theory, and researchers carry out a simulation on classical computers to verify the algorithm of quantum computing. In the near future, quantum computers will jump out of the laboratory, and it will be possible for researchers to perform physical experiments on them [68]–[73]. Current research in quantum computing physics devices is focused on these areas: superconducting quantum computing, semiconductor quantum computing, ion trap quantum computing, atomic quantum computing, nuclear spin quantum computing, and topological quantum computing [74]–[84]. According to current technology and processes, it is still far from being able to be manufactured and run in bulk at room temperature like a classical computer, which indirectly limits the real-world application of quantum computers. Under such a background, based on the principles of these Quantum physical devices, more and more Quantum computing companies and research institutions have released their own Quantum computing cloud platforms, including IBM’s Quantum Experience [85], Rigetti’s Forest [86], and Original Quantum’s computing cloud platform and so on [87].

At present, many researchers are working hard on the physical implementation of quantum computing hardware. When these hardware devices are implemented, it is worthwhile to work image processing on these hardware. All of these efforts are essential to achieve a smooth, effective, and secure QIMP technology so that humans can take full advantage of the great potential of quantum computing. In addition, while realizing

the development of quantum image processing, it is also worth considering how to realize some low-level image and video processing hardware for quantum image processing.

### IV. CONCLUSION

Quantum image processing is a combination of quantum computing and image processing. It is a new thing, and researchers are facing great opportunities and challenges. As an important part of quantum image processing, it is necessary to conduct in-depth research on quantum image representations. This paper introduces and analyzes the latest research results of quantum image representation. Firstly, the general architecture of quantum image processing is given. Then, the various achievements in the field of quantum image representation are discussed, and the similarities and differences in the features and applications of the existing quantum image representation are discussed. Finally, the challenges and future development in the field of quantum image processing are summarized and forecasted. In addition, the work in this paper is valuable as a reference for peer researchers. In the future, we will carry out in-depth research work related to quantum image processing and design efficient quantum image representation models and algorithms.

### REFERENCES

- [1] F. Yan, A. M. Iliyasu, and S. E. Venegas-Andraca, “A survey of quantum image representations,” (in English), *Quantum Inf. Process.*, vol. 15, no. 1, pp. 1–35, Jan. 2016.
- [2] S. E. Venegas-Andraca and S. Bose, “Storing, processing, and retrieving an image using quantum mechanics,” *Proc. SPIE*, vol. 5105, pp. 137–147, Aug. 2003.
- [3] P. Q. Le, F. Dong, and K. Hirota, “A flexible representation of quantum images for polynomial preparation, image compression, and processing operations,” (in English), *Quantum Inf. Process.*, vol. 10, no. 1, pp. 63–84, Feb. 2011.
- [4] P. Q. Le, A. M. Iliyasu, F. Y. Dong, and K. Hirota, “A flexible representation and invertible transformations for images on quantum computers,” in *New Advances in Intelligent Signal Processing*, vol. 372. Springer, Aug. 2011, pp. 179–202. [Online]. Available: [https://link.springer.com/chapter/10.1007%2F978-3-642-11739-8\\_9](https://link.springer.com/chapter/10.1007%2F978-3-642-11739-8_9)
- [5] A. Iliyasu, “Towards realising secure and efficient image and video processing applications on quantum computers,” (in English), *Entropy*, vol. 15, no. 12, pp. 2874–2974, Jul. 2013.
- [6] A. Iliyasu, S. Venegas-Andraca, F. Yan, and A. Sayed, “Hybrid quantum-classical protocol for storage and retrieval of discrete-valued information,” (in English), *Entropy*, vol. 16, no. 6, pp. 3537–3551, Jun. 2014.
- [7] H. Y. Xia, H. Zhang, S. X. Song, H. S. Li, Y. J. Zhou, and X. Chen, “Design and simulation of quantum image binarization using quantum comparator,” (in English), *Mod. Phys. Lett. A*, vol. 35, no. 9, p. 16, Mar. 2020.
- [8] B. Wang, M.-Q. Hao, P.-C. Li, and Z.-B. Liu, “Quantum representation of indexed images and its applications,” (in English), *Int. J. Theor. Phys.*, vol. 59, no. 2, pp. 374–402, Feb. 2020.
- [9] C.-F. Su and C.-Y. Chen, “Information hiding method based on quantum image by using bell states,” (in English), *Quantum Inf. Process.*, vol. 19, no. 1, p. 16, Jan. 2020.
- [10] P. Li, T. Shi, A. Lu, and B. Wang, “Quantum circuit design for several morphological image processing methods,” (in English), *Quantum Inf. Process.*, vol. 18, no. 12, p. 364, Dec. 2019.
- [11] H.-S. Li, S. Song, P. Fan, H. Peng, H.-Y. Xia, and Y. Liang, “Quantum vision representations and multi-dimensional quantum transforms,” (in English), *Inf. Sci.*, vol. 502, pp. 42–58, Oct. 2019.
- [12] H.-S. Li, X. Chen, S. Song, Z. Liao, and J. Fang, “A block-based quantum image scrambling for GNEQR,” (in English), *IEEE Access*, vol. 7, pp. 138233–138243, 2019.



- [13] S. Jiang, R.-G. Zhou, W. Hu, and Y. Li, "Improved quantum image median filtering in the spatial domain," (in English), *Int. J. Theor. Phys.*, vol. 58, no. 7, pp. 2115–2133, Jul. 2019.
- [14] H.-S. Li, Q. Zhu, R.-G. Zhou, L. Song, and X.-J. Yang, "Multi-dimensional color image storage and retrieval for a normal arbitrary quantum superposition state," (in English), *Quantum Inf. Process.*, vol. 13, no. 4, pp. 991–1011, Apr. 2014.
- [15] H.-S. Li, Z. Qingxin, S. Lan, C.-Y. Shen, R. Zhou, and J. Mo, "Image storage, retrieval, compression and segmentation in a quantum system," (in English), *Quantum Inf. Process.*, vol. 12, no. 6, pp. 2269–2290, Jun. 2013.
- [16] S. Yuan, X. Mao, Y. Xue, L. Chen, Q. Xiong, and A. Compare, "SQR: A simple quantum representation of infrared images," (in English), *Quantum Inf. Process.*, vol. 13, no. 6, pp. 1353–1379, Jun. 2014.
- [17] Y. Zhang, K. Lu, Y. Gao, and K. Xu, "A novel quantum representation for log-polar images," (in English), *Quantum Inf. Process.*, vol. 12, no. 9, pp. 3103–3126, Sep. 2013.
- [18] Y. Zhang, K. Lu, Y. Gao, and M. Wang, "NEQR: A novel enhanced quantum representation of digital images," (in English), *Quantum Inf. Process.*, vol. 12, no. 8, pp. 2833–2860, Aug. 2013.
- [19] S. Caraiman and V. Manta, "Image representation and processing using ternary quantum computing," in *Adaptive and Natural Computing Algorithms*, vol. 7824. Springer, Apr. 2013, pp. 366–375. [Online]. Available: [https://link.springer.com/chapter/10.1007%2F978-3-642-37213-1\\_38](https://link.springer.com/chapter/10.1007%2F978-3-642-37213-1_38)
- [20] B. Sun, A. M. Iliyasu, F. Yan, F. Dong, and K. Hirota, "An RGB multi-channel representation for images on quantum computers," *J. Adv. Comput. Intell. Intell. Inform.*, vol. 17, no. 3, pp. 404–417, 2013.
- [21] N. Jiang and L. Wang, "Quantum image scaling using nearest neighbor interpolation," (in English), *Quantum Inf. Process.*, vol. 14, no. 5, pp. 1559–1571, May 2015.
- [22] H.-S. Li, P. Fan, H.-Y. Xia, H.-L. Peng, and S. X. Song, "Quantum implementation circuits of quantum signal representation and type conversion," *IEEE Trans. Circuits Syst. I, Reg. Papers*, vol. 66, no. 1, pp. 341–354, Jan. 2019.
- [23] J. Sang, S. Wang, and Q. Li, "A novel quantum representation of color digital images," (in English), *Quantum Inf. Process.*, vol. 16, no. 2, p. 14, Feb. 2017.
- [24] H.-S. Li, X. Chen, H. Xia, Y. Liang, and Z. Zhou, "A quantum image representation based on bitplanes," (in English), *IEEE Access*, vol. 6, pp. 62396–62404, 2018.
- [25] L. Wang, Q. Ran, J. Ma, S. Yu, and L. Tan, "QRCI: A new quantum representation model of color digital images," (in English), *Opt. Commun.*, vol. 438, pp. 147–158, May 2019.
- [26] N. Zhou, X. Yan, H. Liang, X. Tao, and G. Li, "Multi-image encryption scheme based on quantum 3D arnold transform and scaled zhongtang chaotic system," (in English), *Quantum Inf. Process.*, vol. 17, no. 12, p. 36, Dec. 2018.
- [27] E. Sahin and I. Yilmaz, "QRMW: Quantum representation of multi wavelength images," (in English), *Turkish J. Electr. Eng. Comput. Sci.*, vol. 26, no. 2, pp. 768–779, Mar. 2018.
- [28] K. Liu, Y. Zhang, K. Lu, X. Wang, and X. Wang, "An optimized quantum representation for color digital images," (in English), *Int. J. Theor. Phys.*, vol. 57, no. 10, pp. 2938–2948, Oct. 2018.
- [29] P. C. Li and X. D. Liu, "Color image representation model and its application based on an improved FRQI," (in English), *Int. J. Quantum Inf.*, vol. 16, no. 1, p. 25, Feb. 2018.
- [30] M. Abdolmaleky, M. Naseri, J. Batle, A. Farouk, and L.-H. Gong, "Red-green-blue multi-channel quantum representation of digital images," (in English), *Optik*, vol. 128, pp. 121–132, Jan. 2017.
- [31] R. A. Khan, "An improved flexible representation of quantum images," *Quantum Inf. Process.*, vol. 18, no. 7, p. 201, Jul. 2019.
- [32] X. Liu, D. Xiao, W. Huang, and C. Liu, "Quantum block image encryption based on arnold transform and sine chaotification model," *IEEE Access*, vol. 7, pp. 57188–57199, 2019.
- [33] G. Xu, X. Xu, X. Wang, and X. Wang, "Order-encoded quantum image model and parallel histogram specification," (in English), *Quantum Inf. Process.*, vol. 18, no. 11, p. 346, Nov. 2019.
- [34] L. Wang, Q. Ran, and J. Ma, "Double quantum color images encryption scheme based on DQRCL," *Multimedia Tools Appl.*, vol. 79, nos. 9–10, pp. 6661–6687, Mar. 2020.
- [35] S. E. Venegas-Andraca, "Discrete quantum walks and quantum image processing," Ph.D. dissertation, Univ. Oxford, Oxford, U.K., 2005. [Online]. Available: <https://ora.ox.ac.uk/objects/uuid:2baab08b-ee68-4ce5-8e68-8201f086a1ba>
- [36] M. A. Nielsen and I. L. Chuang, *Quantum Computation and Quantum Information*, 10th ed. Cambridge, U.K.: Cambridge Univ. Press, 2010.
- [37] P. G. Xu, Z. X. He, T. H. Qiu, and M. Hongyang, "Quantum image processing algorithm using edge extraction based on Kirsch operator," (in English), *Opt. Express*, vol. 28, no. 9, pp. 12508–12517, Apr. 2020.
- [38] S. Caraiman and V. Manta, "Image processing using quantum computing," in *Proc. 16th Int. Conf. Syst. Theory, Control Comput. (ICSTCC)*, Oct. 2012, pp. 1–6.
- [39] H.-S. Li, P. Fan, H. Xia, H. Peng, and G.-L. Long, "Efficient quantum arithmetic operation circuits for quantum image processing," *Sci. China Phys., Mech. Astron.*, vol. 63, no. 8, pp. 1–13, Aug. 2020.
- [40] H. Li, *Examining Quantum Algorithms for Quantum Image Processing*. Hershey, PA, USA: IGI Global, 2021, doi: [10.4018/978-1-7998-3799-2](https://doi.org/10.4018/978-1-7998-3799-2).
- [41] M. Nagy and N. Nagy, "Image processing: Why quantum?" (in English), *Quantum Inf. Comput.*, vol. 20, nos. 7–8, pp. 616–626, Jun. 2020.
- [42] J. Luo, R.-G. Zhou, W.-W. Hu, G.-F. Luo, and G. Liu, "Detection of steganography in quantum grayscale images," (in English), *Quantum Inf. Process.*, vol. 19, no. 5, p. 17, Mar. 2020.
- [43] P. Li, T. Shi, Y. Zhao, and A. Lu, "Design of threshold segmentation method for quantum image," (in English), *Int. J. Theor. Phys.*, vol. 59, no. 2, pp. 514–538, Feb. 2020.
- [44] P. Li, T. Shi, A. Lu, and B. Wang, "Quantum implementation of classical Marr–Hildreth edge detection," (in English), *Quantum Inf. Process.*, vol. 19, no. 2, p. 26, Feb. 2020.
- [45] S. X. Jiang, R. G. Zhou, and W. W. Hu, "Quantum image sharpness estimation based on the Laplacian operator," (in English), *Int. J. Quantum Inf.*, vol. 18, no. 3, Apr. 2020, Art. no. 2050008.
- [46] A. M. Grigoryan and S. S. Agaian, "New look on quantum representation of images: Fourier transform representation," (in English), *Quantum Inf. Process.*, vol. 19, no. 5, p. 26, Mar. 2020.
- [47] H.-H. Zhu, X.-B. Chen, and Y.-X. Yang, "A quantum image dual-scrambling encryption scheme based on random permutation," (in English), *Sci. China Inf. Sci.*, vol. 62, no. 12, Dec. 2019, Art. no. 229501.
- [48] R.-G. Zhou, H. Yu, Y. Cheng, and F.-X. Li, "Quantum image edge extraction based on improved prewitt operator," (in English), *Quantum Inf. Process.*, vol. 18, no. 9, p. 24, Sep. 2019.
- [49] R.-G. Zhou and D.-Q. Liu, "Quantum image edge extraction based on improved sobel operator," (in English), *Int. J. Theor. Phys.*, vol. 58, no. 9, pp. 2969–2985, Sep. 2019.
- [50] R.-G. Zhou, Y. Cheng, and D. Liu, "Quantum image scaling based on bilinear interpolation with arbitrary scaling ratio," (in English), *Quantum Inf. Process.*, vol. 18, no. 9, p. 19, Sep. 2019.
- [51] S. Z. Yuan, S. E. Venegas-Andraca, Y. C. Wang, Y. Luo, and X. F. Mao, "Quantum image edge detection algorithm," (in English), *Int. J. Theor. Phys., Article*, vol. 58, no. 9, pp. 2823–2833, Sep. 2019.
- [52] Z. Qu, Z. Li, G. Xu, S. Wu, and X. Wang, "Quantum image steganography protocol based on quantum image expansion and grover search algorithm," (in English), *IEEE Access*, vol. 7, pp. 50849–50857, 2019.
- [53] Z. Qu, Z. Cheng, and X. Wang, "Matrix coding-based quantum image steganography algorithm," (in English), *IEEE Access*, vol. 7, pp. 35684–35698, 2019.
- [54] G. Luo, R.-G. Zhou, and W. Hu, "Efficient quantum steganography scheme using inverted pattern approach," (in English), *Quantum Inf. Process.*, vol. 18, no. 7, p. 24, Jul. 2019.
- [55] A. J. Shields, "Semiconductor quantum light sources," *Nature Photon.*, vol. 1, no. 4, pp. 215–223, Apr. 2007.
- [56] C. Liu and D. Sun, "A Bayesian approach to adaptive video super resolution," in *Proc. CVPR*, Jun. 2011, pp. 209–216.
- [57] F. Y. Shih, *Image Processing and Pattern Recognition (Fundamentals and Techniques)*. New York, NY, USA: Academic, 2010, pp. 306–352. [Online]. Available: [http://www.onacademic.com/detail/journal\\_1000035568756310\\_5805.html](http://www.onacademic.com/detail/journal_1000035568756310_5805.html)
- [58] G. Dougherty, *Digital Image Processing for Medical Applications*. Cambridge, U.K.: Cambridge Univ. Press, 2009.
- [59] S. E. Venegas-Andraca, *Region-Based Approach for the Spectral Clustering Nyström Approximation With an Application to Burn Depth Assessment*. New York, NY, USA: Springer-Verlag, 2015. [Online]. Available: <https://link.springer.com/article/10.1007/s00138-015-0664-3>, doi: [10.1007/s00138-015-0664-3](https://doi.org/10.1007/s00138-015-0664-3).
- [60] V. V. D. Shah, "Image processing and its military applications," *Defence Sci. J.*, vol. 37, no. 4, pp. 457–468, Jan. 1987.
- [61] M. Skolnik, *Radar Handbook*, 3rd ed. London, U.K.: Mendeley, 2008. [Online]. Available: <https://www.mhprofessional.com/9780071485470-usa-radar-handbook-third-edition-group?cat=111>

- [62] N. Varney, Y. Diskin, and V. Asari, "3D object classification in uncalibrated structure from motion models," in *Proc. Imag. Syst. Appl.*, 2015, pp. IW4A-1–IW4A-5.
- [63] M. Lanzagorta, *Quantum Radar*. San Rafael, CA, USA: Morgan & Claypool, 2011.
- [64] M. Mastriani, "Quantum image processing: The pros and cons of the techniques for the internal representation of the image. A reply to: A comment on 'quantum image processing?'" (in English), *Quantum Inf. Process.*, vol. 19, no. 5, p. 156, Mar. 2020.
- [65] R. Singh, H. Parthasarathy, and J. Singh, "Quantum image restoration based on Hudson–Parthasarathy schrodinger equation," (in English), *Quantum Inf. Process.*, vol. 18, no. 11, p. 29, Nov. 2019.
- [66] M. A. M. Sanchez, G.-H. Sun, and S.-H. Dong, "Correlation property of multipartite quantum image," (in English), *Int. J. Theor. Phys.*, vol. 58, no. 11, pp. 3773–3796, Nov. 2019.
- [67] X. Liu, R.-G. Zhou, A. El-Rafei, F.-X. Li, and R.-Q. Xu, "Similarity assessment of quantum images," (in English), *Quantum Inf. Process.*, vol. 18, no. 8, p. 19, Aug. 2019.
- [68] D. Castelvecchi, "Quantum computers ready to leap out of the lab in 2017," (in English), *Nature*, vol. 541, no. 7635, pp. 9–10, Jan. 2017.
- [69] Y. Zhao, X. Chen, Z. Shi, F. Zhou, S. Xiang, and K. Song, "Implementation of one-way quantum computing with a hybrid solid-state quantum system," (in English), *Chin. J. Electron.*, vol. 26, no. 1, pp. 27–34, Jan. 2017.
- [70] H. Xiong, "Multi-level bell-type inequality from information causality and noisy computations," (in English), *Chin. J. Electron.*, vol. 24, no. 2, pp. 408–413, Apr. 2015.
- [71] R. Tenne, U. Rossman, B. Rephael, Y. Israel, A. Krupinski-Ptaszek, R. Lapkiewicz, Y. Silberberg, and D. Oron, "Super-resolution enhancement by quantum image scanning microscopy," (in English), *Nature Photon.*, vol. 13, no. 2, pp. 116–122, Feb. 2019.
- [72] O. S. Magana-Loaiza and R. W. Boyd, "Quantum imaging and information," (in English), *Rep. Prog. Phys., Rev.*, vol. 82, no. 12, Dec. 2019, Art. no. 124401.
- [73] G. Lubin, R. Tenne, I. M. Antolovic, E. Charbon, C. Bruschini, and D. Oron, "Quantum correlation measurement with single photon avalanche diode arrays," (in English), *Opt. Express*, vol. 27, no. 23, pp. 32863–32882, Nov. 2019.
- [74] J. T. Muhonen, J. P. Dehollain, A. Laucht, F. E. Hudson, R. Kalra, T. Sekiguchi, K. M. Itoh, D. N. Jamieson, J. C. McCallum, A. S. Dzurak, and A. Morello, "Storing quantum information for 30 seconds in a nanoelectronic device," *Nature Nanotechnol.*, vol. 9, no. 12, pp. 986–991, 2014.
- [75] M. Veldhorst, C. H. Yang, J. C. C. Hwang, W. Huang, J. P. Dehollain, J. T. Muhonen, S. Simmons, A. Laucht, F. E. Hudson, K. M. Itoh, A. Morello, and A. S. Dzurak, "A two-qubit logic gate in silicon," *Nature*, vol. 526, no. 7573, pp. 410–414, 2015.
- [76] T. F. Watson, S. G. J. Philips, E. Kawakami, D. R. Ward, P. Scarlino, M. Veldhorst, D. E. Savage, M. G. Lagally, M. Friesen, S. N. Coppersmith, M. A. Eriksson, and L. M. K. Vandersypen, "A programmable two-qubit quantum processor in silicon," *Nature*, vol. 555, no. 7698, pp. 633–637, Mar. 2018.
- [77] C. Monroe and J. Kim, "Scaling the ion trap quantum processor," *Science*, vol. 399, no. 6124, pp. 1164–1169, 2013.
- [78] V. M. Schafer, C. J. Ballance, K. Thirumalai, L. J. T. G. Stephenson, A. M. Steane, and D. M. Lucas, "Fast quantum logic gates with trapped-ion qubits," *Nature*, 2018.
- [79] J.-M. Cui, Y.-F. Huang, Z. Wang, D.-Y. Cao, J. Wang, W.-M. Lv, L. Luo, A. D. Campo, Y.-J. Han, C.-F. Li, and G.-C. Guo, "Experimental trapped-ion quantum simulation of the Kibble-Zurek dynamics in momentum space," *Sci. Rep.*, vol. 6, no. 1, p. 33381, Dec. 2016.
- [80] M. H. Devoret and R. J. Schoelkopf, "Superconducting circuits for quantum information: An outlook," *Science*, vol. 339, no. 6124, pp. 1169–1174, Mar. 2013.
- [81] D. S. Weiss and M. Saffman, "Quantum computing with neutral atoms," *Phys. Today*, vol. 70, no. 7, pp. 44–50, Jul. 2017.
- [82] H. Bernien, S. Schwartz, A. Keesling, H. Levine, A. Omran, H. Pichler, S. Choi, A. S. Zibrov, M. Endres, M. Greiner, V. Vuletic, and M. D. Lukin, "Probing many-body dynamics on a 51-atom quantum simulator," *Nature*, vol. 551, no. 7682, pp. 579–584, Nov. 2017.
- [83] N. A. Gershenfeld and I. L. Chuang, "Bulk spin-resonance quantum computation," *Science*, vol. 275, no. 5298, pp. 350–356, Jan. 1997.
- [84] A. Stern and N. H. Lindner, "Topological quantum computation—from basic concepts to first experiments," *Science*, vol. 339, no. 6124, pp. 1179–1184, Mar. 2013.
- [85] IBMQ. *IBM Quantum Experience*. Accessed: Sep. 21, 2020. [Online]. Available: <https://quantum-computing.ibm.com/>
- [86] Rigetti Forest. *Rigetti Quantum Cloud Services platform*. Accessed: Sep. 21, 2020. [Online]. Available: <https://www.rigetti.com/>
- [87] *Original Quantum. Original Quantum's Computing Cloud Platform*. Accessed: Sep. 21, 2020. [Online]. Available: <http://www.qubitonline.cn/>



**JIE SU** received the M.S. degree in mathematics and computer science from Yunnan Minzu University, in 2016. He is currently pursuing the Ph.D. degree with the College of Information and Electrical Engineering, China Agricultural University, Beijing, China. His research interests include natural language processing, pattern recognition, quantum information processing, image processing, and machine learning.



**XUCHAO GUO** received the bachelor's degree in computer science and the master's degree from Shandong Agricultural University, Tai'an, China, in 2015 and 2018, respectively. He is currently pursuing the Ph.D. degree with the College of Information and Electrical Engineering, China Agricultural University, Beijing, China. His research interests include complex network analysis, data mining, natural language processing, knowledge graph, machine learning, and image processing.



**CHENGQI LIU** received the master's degree from China Agricultural University, Beijing, China, in 2018, where he is currently pursuing the Ph.D. degree. His research interests include image processing and deep learning for video processing.



**LIN LI** is currently a Professor and a Doctoral Supervisor with the College of Information and Electrical Engineering (CIEE), China Agricultural University. Her main research interests include knowledge engineering and machine learning.

• • •